NAVWEPS REPORT 7395

THE AERODYNAMIC DESIGN OF AXISYMMETRIC NOZZLES FOR HIGH-TEMPERATURE AIR

5 FEBRUARY 1962

U. S. NAVAL ORDNANCE LABORATORY
WHITE OAK, MARYLAND

NAVWEPS 7395

NAVWEPS REPORT 7395

Aeroballistics Research Report No. 137

THE AERODYNAMIC DESIGN OF AXISYMMETRIC NOZZLES FOR HIGH-TEMPERATURE AIR

by

K. R. Enkenhus and E. F. Maher.

ABSTRACT: A method is given for designing contoured axisymmetric nozzles for a shock tunnel or an arc-heated wind tunnel, in which the supply air temperature is high enough to produce real-gas effects. The formulation is based on the assumption that the air undergoes an isentropic expansion while remaining in thermodynamic equilibrium.

The isentropic core contour is determined by solving the inviscid flow equations by the method of characteristics. The turbulent boundary-layer growth and the convective heat-transfer rate to the nozzle wall are found from a numerical integration of the momentum integral equation, together with the application of Reynolds analogy. The properties of high-temperature air are introduced in the form of empirical formulas based on the thermodynamic data of the National Bureau of Standards, and the transport properties of Hansen (NACA TN 4150). The design method has been coded on an IBM 704 computer and has been used to investigate the performance characteristics of a family of hypervelocity nozzles having exit Mach numbers from 11 to 19 for supply pressures from 50 to 500 atmospheres and supply temperatures up to 7500°K.

Examples are given of nozzle contours, and charts are supplied for the determination of the principal dimensions (throat size, length, etc.) of high-temperature nozzles having a selected maximum flow expansion angle. Information is also given for establishing the nozzle supply conditions, weight flow and air heating power required to sustain the desired test-section conditions. From the boundary-layer calculations, simple

PUBLISHED MARCH 1962

[redacted] NAVAL ORDNANCE LAB[redacted]
WHITE OAK, [redacted]

expressions were obtained which correlate, over a wide range of conditions, the nozzle exit turbulent boundary-layer displacement thickness, and the peak convective heat-transfer ra e occurring in the vicinity of the throat. It was found that the values of the boundary-layer momentum thickness Reynolds number were high enough to make the assumption of a turbulent boundary layer reasonable under most operating conditions of interest.

5 February 1962

A necessary part of the development program for high-speed vehicles consists of the testing of models in ground facilities in order to obtain basic aerodynamic design data. Examples of these ground facilities are the shock tunnel and the arc-heated wind tunnel. In both types of facilities, the high temperature of the flow causes the air to depart markedly from the behavior of a perfect gas due to chemical reactions such as the dissociation of oxygen and nitrogen, and the formation of nitric oxide. The need has therefore arisen to develop a method of designing nozzles which is not limited to the case of a perfect gas. The present report describes a method developed at this Laboratory for aerodynamically designing axisymmetric nozzles on a high-speed computer employing the thermodynamic and transport properties of high-temperature equilibrium air.

This work is one phase of a comprehensive program investigating the problems associated with high-speed flight and its simulation. The investigation was supported by the Bureau of Naval Weapons under Task No. PR-10.

The authors wish to acknowledge the contribution of Mr. J. R. Powers, who performed the analysis in Appendix C. They also extend their thanks to Dr. M. Grabau of the Arnold Engineering Development Center for his co-operation in supplying refined coefficients for the curve fit formulas for the thermodynamic properties of air.

W. D. COLEMAN
Captain, USN
Commander

FLORIAN GEINEDER
By direction

CONTENTS

ILLUSTRATIONS

TABLES

SYMBOLS

a	sound speed
A	area
C_f	skin-friction coefficient = $2\tau_w/\rho_\infty u_\infty^2$
c_p	heat capacity at constant pressure
h	enthalpy
h_D	dissociation enthalpy per unit mass in the free stream
L	nozzle throat-to-exit length
Le	Lewis number
M	Mach number
N	exponent in velocity profile law (equation (25))
p	pressure
Pr	Prandtl number
q	total velocity
q_H	convective heat-transfer rate per unit area
Q	power required to heat air per unit test-section area
r	radial co-ordinate
R	gas constant for air
R_c	nozzle throat radius of curvature
Re_x	Reynolds number based on length x = $\frac{\rho_\infty u_\infty x}{\mu_\infty}$
Re_{crit}	Reynolds number of laminar instability
Re_{min}	minimum Reynolds number at which turbulent flow can exist
s	distance along isentropic core boundary
S	entropy

St	Stanton number
T	temperature
u	axial velocity (in characteristics equations) or velocity component parallel to wall (in boundary-layer equations)
u_τ	friction velocity
v	velocity component normal to u component
w	weight flow rate per unit test-section area
x	axial co-ordinate
x_t	distance from nozzle throat to start of test cone
y	distance from origin of radial source flow (or, distance normal to wall)
Z	compressibility
γ	ratio of specific heats
δ	boundary-layer velocity thickness
δ^*	boundary-layer displacement thickness
θ	boundary-layer momentum thickness
Θ	Prandtl-Meyer angle
μ	viscosity
$\bar{\mu}$	Mach angle
ν	kinematic viscosity
ξ_i	parameters which influence the skin-friction coefficient
ρ	density
τ	shear stress
ϕ	velocity potential
ω	nozzle expansion half-angle (see Figure 30)

Subscripts

ad	adiabatic wall value

c	condensation threshold value
e	nozzle exit condition
o	supply condition
ref	value at reference enthalpy
w	wall value
∞	free-stream value
*	nozzle throat condition

Superscript

+	denotes length made dimensionless by dividing by r_e

THE AERODYNAMIC DESIGN OF AXISYMMETRIC NOZZLES FOR HIGH-TEMPERATURE AIR

INTRODUCTION

A computer program for the design of perfect-gas nozzles was developed at the U. S. Naval Ordnance Laboratory several years ago. The inviscid core was calculated by the method of characteristics (reference (a)) and then a turbulent boundary-layer correction was added to obtain the final nozzle contour (reference (b)). The program has been very satisfactory for perfect-gas nozzles. However, when interest is focused on hypervelocity nozzles with elevated stagnation temperatures the assumption of perfect-gas behavior is not even approximately valid. The objective of the present work is to take into account the real-gas effects in such flows. Basically, the method is an extension of the work described in references (a) and (b) where now the properties of high-temperature air replace the perfect-gas relations, both in calculating the isentropic core and the turbulent boundary-layer correction.

ANALYSIS

Assumptions

The method derived here assumes the air undergoes an isentropic expansion in the core while remaining in local thermodynamic equilibrium in both the core and boundary layer. Although the assumption of equilibrium flow is a valid approximation for a wide range of conditions of interest in hypervelocity nozzles, the extent to which this approximation is justifiable should be determined for each case.

When high-temperature air is expanded to the ambient temperatures occurring in the atmosphere, the finite recombination rate of the atoms leads to non-equilibrium flow. This is due to the fact that the recombination rate, which is strongly dependent on the local temperature and pressure, falls by several orders of magnitude during the expansion process. At some point in the nozzle the recombination rate invariably becomes so low that the chemical constitution of the flow "freezes" in a mixture with a higher concentration of atomic species than would occur if the flow had expanded in equilibrium.

While in general both oxygen and nitrogen recombination rates must be taken into account, the degree of dissociation of nitrogen is negligible if the supply temperature is less than 5000°K (reference (c)). The effect of a finite oxygen recombination rate on the one-dimensional flow of a gas approximating air has been theoretically studied (reference (d)). As an example of the results, the fraction of oxygen by weight which freezes in a representative conical hypervelocity nozzle (test-section Mach number = 15, length 6 ft) is shown as a function of supply temperature and pressure in Figure 1. The effect is most serious at low air supply densities, i.e., high supply temperatures and low pressures. The results of Figure 1 may be used as a guide for estimating the seriousness of non-equilibrium flow effects for any hypervelocity nozzle, since it was found that the fraction of oxygen which freezes in atomic form is governed primarily by the supply conditions, and is only weakly dependent on the exit Mach number and the nozzle length and geometry.

The study further indicated that when the amount of oxygen which freezes is less than a few percent, the resulting departure of the flow parameters from their equilibrium values is small enough to make the assumption of equilibrium flow justifiable.

Non-equilibrium flow may also result from the finite vibrational relaxation time of molecules. However, the energy associated with this mode is relatively small compared with the energy in dissociation, so that vibrational relaxation effects may be expected to be small in comparison to the effects resulting from a finite recombination rate.

In addition to making an assumption about the thermodynamic state of the flow, it is necessary to reach some conclusion as to whether the boundary layer on the nozzle walls will be laminar or turbulent. The usual situation is for a turbulent boundary layer to exist, except in low density wind-tunnel nozzles, which are operated with a supply pressure which is only a small fraction of an atmosphere. Since experimental data for high-temperature nozzles are not yet available, it is necessary to draw conclusions about the probable state of the boundary layer from theory and from the available experimental measurements. While moderate wall cooling tends to stabilize the boundary layer (reference (e)), the wall-to-free-stream temperature ratios in hypervelocity nozzles are low enough to fall into the region of extreme wall cooling for which rather low transition Reynolds numbers have been reported (references (f) and (g)). For example, it was found in reference (g) that transition took place on the cylindrical portion of a hemisphere cylinder at a momentum thickness Reynolds number, Re_θ, which varied from 400 to 625 as the wall-to-stagnation enthalpy ratio was decreased from 1/9 to 1/30.

The momentum thickness Reynolds numbers near the throat of the family of hypervelocity nozzles investigated in this report was computed to be generally much larger than those for which transition was observed to occur on the cylindrical portion of a hemisphere-cylinder in the tests described in reference (g). Values of Re_θ from 430 to 16,000 were obtained for the turbulent boundary layer at the throat of nozzles designed for exit Mach numbers from 11 to 19, with supply temperatures of 2500°K to 7500°K, and supply pressures from 50 to 500 atmospheres. The existence of a turbulent boundary layer, at least at and downstream of the throat, is therefore highly probable in the majority of cases. For the sake of simplicity, and also to obtain an estimate of the maximum throat heat-transfer rate, it was assumed in the calculations that the boundary layer is fully turbulent everywhere.

Nozzle Supply Parameters

The first step in the design of a nozzle is the determination of the air supply temperature and pressure necessary to achieve the desired test-section conditions. The corresponding values of the weight flow and air heating power required to sustain operation must also be found.

Although for sufficiently elevated supply conditions real-gas effects must be taken into account in the expansion process, for duplication of temperatures in the atmosphere, the final state of the air in the test section will always lie in the perfect-gas regime. For an adiabatic expansion the supply enthalpy is equal to the total enthalpy of the air in the test section, which for low enough test-section temperatures is given by the perfect-gas relation

$$h_o = c_p T_e \left(1 + \frac{\gamma - 1}{2} M_e^2\right) . \tag{1}$$

The entropy of the flowing air is assumed to be constant and is equal to the value in the test section. Its value, made dimensionless by dividing by the gas constant R, is

$$S/R = (c_p/R)\ln(T_e/T_1) - \ln(p_e/p_1) + S_1/R \tag{2}$$

where S_1/R = 23.588 at T_1 = 273.16°K and p_1 = one atmosphere. For given test-section conditions, the supply enthalpy and entropy can be computed using equations (1) and (2). These quantities in turn may be used to determine the supply temperature and pressure through the use of a Mollier chart for high-temperature air (e.g., references (c) or (h)).

The two extremes of test conditions bounding the operational range of interest are those of "true-temperature" and "condensation-threshold" operation. The former refers to a test environment temperature identical to that encountered in free flight. Condensation-threshold conditions refer to a test-section temperature just sufficient to avoid liquifaction of the air at the prevailing pressure. For true-temperature conditions the supply pressure is shown as a function of the nozzle exit Mach number in Figure 2, for a range of static pressures from 0.01 to 1 mm Hg. The curves are calculated for a test-section static temperature of 222°K (400°R), which is a mean value for the ambient temperature in the upper atmosphere.

From Figure 2 it can be seen that for true-temperature operation, the highest Mach number which can be obtained with a desirable test-section static pressure rapidly approaches a practical limit due to the excessive supply pressures required. Considerably higher Mach numbers can be obtained for the same supply and exit static pressures by operating at the condensation threshold. The supply pressure required for condensation-threshold operation is shown as a function of test-section Mach number and static pressure in Figure 3.

The condensation temperature used to obtain the results shown was calculated from the formula of reference (i),

$$T_c = \frac{336.36}{6.995 - \log_{10} p_e} \tag{3}$$

which assumes no super-cooling. The units in equation (3) are degrees Kelvin and millimeters of mercury. The condensation temperature is plotted as a function of pressure in Figure 4.

A direct comparison of the supply pressure requirements versus Mach number for true-temperature and condensation-threshold operation is shown in Figure 5. The test-section static pressure is assumed to be 0.1 mm Hg. The dotted curve shows the supply pressure which would be required if the air behaved as a perfect gas with $\gamma = 1.4$. It will be noted that at Mach 15 the supply pressure required for true-temperature operation is approximately seven times greater than for condensation-threshold operation. At high Mach number the supply pressure needed for condensation-free operation is a little higher than that calculated by the perfect-gas formula, due to the fact that the supply temperatures are high enough to result in some real-gas effects.

The supply temperatures necessary for true-temperature and condensation-threshold operation are shown in Figures 6 and 7, respectively. A comparison of supply temperature requirements versus Mach number is shown in Figure 8 for true-temperature operation with a perfect gas and with equilibrium air, and for condensation-threshold operation with equilibrium air. The test-section static pressure is again taken to be 0.1 mm Hg. For true-temperature operation, the supply temperature calculated by the perfect-gas formula is, of course, much larger than the correct value because the storage of energy in the dissociative and vibrational modes is not taken into account. The supply temperature for condensation-threshold operation is seen to be rather modest compared with the true-temperature operating requirements.

The weight flow rate in the nozzle per unit test-section area may be expressed in terms of test-section conditions by the perfect-gas formula

$$w = g\rho_e u_e = g p_e M_e \left(\frac{\gamma}{RT_e}\right)^{\frac{1}{2}} . \tag{4}$$

The air heating power required per unit test-section area (assuming that the air is heated for an initial temperature T_e) is

$$Q = \frac{1}{2}\rho_e u_e^3 = \frac{1}{2}\gamma^{3/2}(RT_e)^{1/2} p_e M_e^3 \tag{5}$$

The weight flow and air heating power for operation with a test-section static temperature of 293°K are shown in Figures 9 and 10, respectively. The corresponding values at any other exit temperature may be found by multiplying equation (4) or dividing equation (5) by the factor

$$\sqrt{293/T_e} .$$

Design of the Inviscid Supersonic Core

a. Characteristic Equations

The method employed in designing the inviscid core is an extension to the real-gas case of a procedure developed previously for perfect-gas nozzles (reference (a)).

The axisymmetric, isentropic, irrotational flow of a fluid satisfies the potential equation

$$\left(1 - \frac{\phi_x^2}{a^2}\right)\phi_{xx} + \left(1 - \frac{\phi_r^2}{a^2}\right)\phi_{rr} - \frac{2\phi_x\phi_r}{a^2}\phi_{xr} + \frac{\phi_r}{r} = 0 \qquad (6)$$

where $-\phi_x = u, \quad -\phi_r = v$.

This equation is derivable from the laws of continuity and momentum and, therefore, is independent of the equation of state of the fluid. It therefore holds for high-temperature air as well as for a perfect gas. For supersonic flow, the equation is hyperbolic and can be solved by the method of characteristics. The **slopes** of the two families of characteristic lines (which correspond to the Mach waves in the flow) are given by

$$\left(\frac{dr}{dx}\right)_{\pm} = -\left\{uv \pm a\left[(u^2+v^2)-a^2\right]^{1/2}\right\} \Big/ (a^2-u^2) \qquad (7)$$

where the plus sign refers to the right-running family of characteristic lines and the minus sign refers to the left-running family (see Figure 11a). The variations of the axial and radial velocity components along the characteristic lines are given by the expressions

$$\frac{du}{dx} + \left(\frac{dr}{dx}\right)_{\pm} \cdot \frac{dv}{dx} = \frac{v a^2}{r} \qquad (8)$$

The particular method employed here to solve the characteristic equations is a lattice-point technique described by Cronvich (reference (j)). By this method, given the flow conditions at the neighboring points 1 and 2 (Figure 11a), the location and flow variables of another point 3 can be determined. Such a point lies at the intersection of the two characteristic lines (of different families) passing through points 1 and 2. This is accomplished by use of the characteristic equations (7) and (8) in finite-difference form. These finite-difference forms comprise four equations in the five unknowns x, y, u, v, and a at point 3. The fifth equation needed to determine a unique solution is provided by an expression for the speed of sound in air as a function of the local flow velocity, to be described later.

b. The Characteristics Solution

To begin the calculation, the flow conditions must be known along some bounding curve. In this case (see Figure 11b), the boundary is chosen as the nozzle axis AC and the terminal Mach line CD which forms the upstream limit of the test cone. For the assumed equilibrium isentropic expansion of air from given supply conditions the flow variables can be considered as unique functions of Mach number. If these functions are known then the flow can be completely specified by a knowledge of the Mach number distribution. In the present method, in order to obtain the required initial data along the boundary a Mach number distribution is assigned along the axis and the other flow variables are obtained by appropriate real-gas relations.

The construction of the characteristic net begins at a point B on the axis downstream of the throat at which the Mach number is slightly greater than one, but not too close to one, since convergence difficulties may be encountered due to the steep slope of the Mach lines in this region. Knowledge of the flow conditions along the boundary BCD is sufficient to determine the characteristic net in the region above the boundary enclosed by the left characteristic passing through B and the right characteristic through D. Thus, the construction proceeds along and outward from the axis toward the wall position, which is yet to be determined. To locate the wall streamline the equation for continuity of weight flow is numerically integrated along a characteristic line. In order to do this, the density must be known as a function of the local flow velocity. The construction of a characteristic is continued until the total weight flow exceeds that through the exit. At the exit, where by design the flow is uniform, the total weight flow is $w = g\rho_e q_e A_e$. The wall is then located by interpolation between the last mesh points on the characteristic line such as to satisfy the continuity of mass flow.

It is seen that the first wall point that can be calculated downstream of the throat (point E, Figure 11b) is determined by the curved Mach line passing through the initial axis point B. The throat wall point F can be determined by the continuity of mass flow relation if it is assumed that the flow is one-dimensional here, i.e.,

$$r_* = \left(\frac{w}{g\pi\rho_* q_*}\right)^{1/2} \qquad (9)$$

This leaves a gap EF along which the position of the wall contour is not determined. However, in the present work, it has been found that the gap thus created is quite small for exit Mach numbers greater than five. Therefore, the calculated contour is faired into the throat without resorting to a perturbation solution in the region of the throat as was done, for example, by Owen and Sherman (reference (k)) for lower Mach number, perfect-gas nozzles.

c. Inclusion of Real-Gas Properties

In general, it would be most convenient to have expressions for the sound speed and density in terms of the enthalpy and entropy, i.e.,

$$a = a(h,S)$$

$$\rho = \rho(h,S).$$

The reason for this is that for an isentropic process S is constant, and h may be expressed in terms of velocity by the energy equation

$$h + q^2/2 = h_0 = \text{constant} . \tag{10}$$

The expressions for a and ρ can therefore be considered as functions of q alone for a given set of supply conditions. Thus, given a Mach number distribution along the axis, the equation $M = q/a(q)$ can be iterated upon to provide corresponding values of velocity and sound speed on the boundary. This value of q in turn determines the density needed in the weight flow calculation. For all off-axis points, the equations provide the necessary relations between a, ρ, and q to determine the position of the characteristic lines and the weight flow across them.

However, existing expressions for the thermodynamic properties of air are not in the above form and thus necessitate a different approach to the problem. In reference (l) there are given three empirical equations for the compressibility, entropy, and enthalpy of equilibrium air as functions of pressure and density, based on the thermodynamic properties of air as calculated by the National Bureau of Standards (reference (m)). These equations are of the form

$$z = f_1(p, \rho) \tag{11}$$

$$S/R = f_2(p, e) \tag{12}$$

$$he/p = f_3(p, e) \quad . \tag{13}$$

When the pressure, density, and compressibility are known, the temperature may be found from the equation of state

$$p = Z\rho RT \quad . \tag{14}$$

A fifth equation for the sound speed was obtained by differentiating equation (12), resulting in

$$a = \left[\left(\frac{\partial p}{\partial \rho}\right)_S\right]^{\frac{1}{2}} = f_4(p, e) \quad . \tag{15}$$

In the form given in reference (l), the accuracy of equations (12) and (13) was not sufficient for the present purpose. The differences between the values calculated using equations (12) and (13) and those tabulated in reference (m) were plotted and fitted locally by quadratics. The coefficients of these quadratics are supplied to the computer for an error correction to the original equations. The resulting expressions for the thermodynamic properties of air are extremely lengthy and therefore are not listed here. The average error of these expressions with respect to the tabulated values of reference (m) ranges from a fraction of a percent for entropy and compressibility to about two percent for enthalpy and sound speed.

For a given supply temperature and pressure, the inviscid core flow field and its contour can be obtained by a solution of the characteristic equations (7) and (8) in conjunction with equations (10) to (15). This involves an iteration of the characteristic and thermodynamic equations at each boundary and mesh point.

The necessity of obtaining a simultaneous solution of the lengthy thermodynamic property equations for each iteration at every mesh point was avoided by constructing an isentropic flow table of corresponding values of all the pertient variables for the given stagnation conditions over the desired Mach number range. The table is constructed as follows: for a given supply pressure and temperature the supply density is found by performing an iteration on equations (11) and (14). Once the density is obtained, the initial entropy and all the other supply conditions can be determined from the knowledge of p and ρ. Then the pressure, p, is decremented as the independent variable. For each value of p, an iteration for ρ is performed on equation (12) until the condition $S = S_0$ is satisfied. Once again, knowing p and ρ, all the other thermodynamic properties can be calculated by equations (11) through (15). The Mach number can also be obtained by the use of equation (10). The table is complete when p has been decremented until the desired exit Mach number is reached. The table is then stored on tape and read into the computer when needed. In the table are included corresponding values of the Mach number, sound speed, density, and enthalpy (or velocity from equation (10)) required for the characteristics solution and wall contour determination. Also included are the values of pressure, compressibility, and the one-dimensional area ratio $A/A_* = \frac{\rho_* u_*}{\rho u}$.

The latter quantities are required for the subsequent boundary-layer calculations and for determining the subsonic inlet flow.

The isentropic table obtained in this manner allows the determination of all of the flow parameters by interpolation, upon specifying any one of them. Thus specification of a Mach number distribution along the axis also defines the remaining flow variables along this boundary. The tables also supply the relation between velocity and sound speed needed as a fifth equation for the finite-difference solution to the characteristic equations. Likewise, density is defined as a function of velocity and can be supplied for the computation of the weight flow.

d. Axial Mach Number Distribution

In order to specify the flow conditions along the boundary there are many Mach number distribution functions, M(x), that can be chosen. A smooth function is required satisfying the conditions $M(0) = 1$, $M(x_t) = M_e$, and $M'(x_t) = 0$. The number of constants in the function is determined by how many independent parameters the designer wishes to choose. A satisfactory function (similar to that described in reference (k)) is

$$M(x) = M_e - C_1 \left(e^{C_2 (x - x_t)^2} - 1 \right) \qquad (16)$$

where C_1 and C_2 are constants. Equation (16) automatically satisfied the conditions $M(x_t) = M_e$ and $M'(x_t) = 0$. The two constants C_1 and C_2 are determined by imposing two other boundary conditions. One, as mentioned above, is that $M(0) = 1$. The second consists of the specification of the axial derivative of the Mach number at the throat, i.e., $M'(0)$.

e. Basic Nozzle Dimensions

Since the potential core may be scaled to any size, it is convenient to make all lengths dimensionless by dividing by the exit radius r_e, and to denote such quantities by a (+) sign. The values of M_e, x_t+ and $(dM/dx^+)_{x^+ = 0}$ determine the maximum half expansion angle ω of the nozzle and the throat-to-exit length L^+. The value of $(dM/dx^+)_{x^+ = 0}$ further governs the contour radius of curvature at the throat.

The value of ω resulting from a particular choice of the initial parameters is of importance due to the possibility of flow separation associated with too large a value of the expansion angle. In practice, it is desirable to have a value of ω of about 10^o to avoid any possibility of separation. Although larger values of ω would appear desirable in helping to reduce the relatively great length of high Mach number nozzles, increasing the expansion angle is not an effective method for reducing nozzle length since at high Mach numbers the major portion of the nozzle is taken up in straightening out the flow after the initial expansion. (This is illustrated in Figure 16 which shows the nozzle contours and inviscid cores for two representative hypervelocity nozzles.) Since the exact value of ω can only be determined after the computation of the wall co-ordinates, approximate relationships between ω, M_e, x_t^+ and $(dM/dx^+)_{x^+ = 0}$ are desirable so that a computation will not be invalidated due to separation problems resulting from a poor choice of the initial parameters. To accomplish this, the perfect gas nozzle design method of Foelsch (reference (n)) may be applied to obtain the values of x_t^+ and $(dM/dx^+)_{x^+ = 0}$ corresponding to some chosen value of ω and M_e. The method is outlined in Appendix A where it is shown that simple perfect-gas relations exist in the form

$$x_t^+ = f_1(M_e, \omega) \tag{17}$$

$$(dM/dx^+)_{x^+=0} = f_2(M_e, \omega) \quad . \tag{18}$$

The use of these values to determine the constants in the axial Mach number distribution selected for the real-gas computation (equation (16)) leads, after the solution by the method of characteristics, to a real-gas nozzle of approximately the same expansion angle. It should be emphasized that no perfect-gas assumption is being employed here. The perfect-gas equations (17) and (18) are used only as a guide in prescribing the constants of the imposed Mach number distribution. Thereafter, a real-gas nozzle core is calculated so as to generate this chosen distribution. It might be added that the difference between the value of ω assumed in equations (17) and (18) and the value determined by the wall co-ordinates in the resultant real-gas calculation is of the order of 1°.

For guidance in the determination of the initial parameters, plots have been made from the Foelsch equations for a family of nozzles with expansion angles of 5°, 10°, and 15°. Figures 12 and 13 show values of x_t^+ and $(dM/dx^+)_{x^+=0}$ as functions of exit Mach number. Figure 14 gives the dimensionless nozzle length from throat to exit, $L^+ = x_t^+ + \cot\bar{\mu}_e$.

f. Throat Radius of Curvature

For the design of a subsonic inlet to match the supersonic contour, the radius of curvature at the throat, R_c, is needed. For the perfect-gas case, assuming one-dimensional flow, R_c can be simply expressed in terms of $r*$ and the axial derivative of the Mach number $M'(0)$. (See equation (B-7) of Appendix B.) The Mach number derivative can easily be obtained from the assigned distribution $M(x)$.

A simple analytic form does not exist for the real-gas case. However, a numerical procedure can be used to obtain a value of R_c from the isentropic table discussed previously, although the accuracy of such a method is limited. A discussion of the perfect- and real-gas relations for the throat radius of curvature is given in Appendix B.

Design of the Inviscid Subsonic Core

a. Contour Shape

A smooth subsonic inlet shape $r(x)$ is required which will possess zero slope at the throat while matching the radius of curvature there as determined in the supersonic calculations. These conditions may be expressed $r(0) = r_*$, $r'(0) = 0$, $r''(0) = 1/R_c$.

The conditions given above are sufficient to define the parabola

$$r = r_* + \frac{x^2}{2R_c} \quad . \tag{19}$$

The parabolic inlet was only used for a few exploratory calculations since this contour is unnecessarily long. A cubic inlet was used for most of the calculations. In order to determine this cubic another condition must be imposed besides those listed above. This is provided by specifying an arbitrary contour point (x_A, r_A) upstream of the throat. Then the inlet contour is given by

$$r = \left(r_A - r_* - \frac{x_A^2}{2R_c}\right)\frac{x^3}{x_A^3} + \frac{x^2}{2R_c} + r_* \quad . \tag{20}$$

b. Flow Calculation

The flow parameters along the subsonic wall streamline are needed for the subsequent boundary-layer calculations. By assuming the flow to be one-dimensional, all the necessary flow quantities may be obtained from the isentropic expansion table. For each of the area ratios tabulated the corresponding axial distance x is defined by equations (19) or (20).

Turbulent Boundary-Layer Correction

In order to obtain the final nozzle contour, a boundary-layer correction equal to the boundary-layer displacement thickness is added to the isentropic core co-ordinates. It has been indicated that the boundary layer will probably be turbulent for most of the operating conditions of interest.

In formulating a method for computing turbulent boundary-layer growth in a high-temperature flow, there are three main factors which must be taken into account: the change in the thermodynamic and transport properties of air which occurs at high temperatures, the diffusion of atomic species which recombine and release additional heat to the wall, and the effect on skin friction and heat transfer of a highly cooled wall. At the present time, a fundamental theoretical approach to the problem is not possible since the basic mechanisms of the turbulent boundary layer are not understood even for low-temperature flow. It is necessary to extend the existing low-temperature, semi-empirical theories to high temperatures. Since very little data for high-temperature flows are available, the results must be treated with some reservations.

The method employed here consists of integrating the von Karman momentum integral equation

$$\frac{d\theta}{ds} = C_f/2 - \theta\left[\left(2+\frac{\delta^*}{\theta}\right)\frac{1}{u_\infty}\frac{du_\infty}{ds} + \frac{1}{\rho_\infty}\frac{d\rho_\infty}{ds} + \frac{1}{r}\frac{dr}{ds}\right] \qquad (21)$$

along the nozzle contour to obtain the boundary-layer momentum thickness θ. The shape parameter δ^*/θ appearing in the equation is found from

$$\delta^*/\theta = \frac{\delta^*/\delta}{\theta/\delta} \qquad (22)$$

where, by definition,

$$\delta^*/\delta = \int_0^1 \left(1 - \frac{\rho u}{\rho_\infty u_\infty}\right) d(y/\delta) \qquad (23)$$

and

$$\theta/\delta = \int_0^1 \frac{\rho u}{\rho_\infty u_\infty}\left(1 - \frac{u}{u_\infty}\right) d(y/\delta) \; . \qquad (24)$$

To evaluate these integrals, the variation of velocity and density in the boundary layer must be specified. A power-law velocity profile

$$\frac{u}{u_\infty} = (y/\delta)^{\frac{1}{N}} \qquad (25)$$

was assumed, with N given by the empirical formula

$$N = 2.05 \log_{10} R_{e_\theta} - 1.65 \; . \qquad (26)$$

This formula is based on experimental measurements in supersonic turbulent boundary layers at low temperatures (see

Figure 3 of reference (o)). Equation (26) agrees with available experimental data at large value of Re_θ, and has the desired property of making N approach unity (i.e., a laminar type profile) at low values of Re_θ. Some more recent experimental data (reference (p)) seems to indicate, however, that the value of N rises rapidly downstream of the transition point to a value of 7 to 12, falls a little, and then begins a monotonic increase as described by equation (26).

Although a power-law velocity profile is valid only in the outer turbulent layer, the formula may be satisfactorily applied to the entire boundary layer when evaluating equations (23) and (24), under the assumption that the laminar sublayer is thin.

In order to obtain the density in the boundary layer, it is first necessary to derive a relation for the enthalpy. The Crocco relation was employed in the modified form

$$h = h_w + (h_{ad} - h_w)\frac{u}{u_\infty} - (h_{ad} - h_\infty)\left(\frac{u}{u_\infty}\right)^2 \qquad (27)$$

where

$$h_{ad} = h_\infty + P_r^{1/3}(h_o - h_\infty) \qquad (27a)$$

The density in the boundary layer is then found from a relation for high-temperature air in thermodynamic equilibrium,

$$\rho = \rho\,(p_\infty, h) \qquad (28)$$

obtained by an iterative solution of equation (13).

To complete the specification of quantities appearing in the momentum integral equation, an empirical formula must be employed for the skin-friction coefficient, which is of the form

$$c_f = c_f\,(R_{e_\theta}, \xi_i) \qquad (29)$$

where Re_θ is the Reynolds number based on the boundary-layer momentum thickness, and the parameters ξ_i (i = 1, 2, ...) may include free-stream conditions, wall temperature, and in some formulas, a factor allowing for the influence of local pressure gradient. The formulas which were employed in the calculations are given in Appendices C and D.

The convective heat-transfer rate* to the surface is

$$q_H = \rho_\infty u_\infty St\,(h_{ad} - h_w) \tag{30}$$

The Stanton number was computed using Colburn's version of Reynolds analogy, multiplied by a factor involving the Lewis number to account approximately for the effect of diffusion in the boundary layer, as suggested in reference (r).

$$St = \frac{C_f}{2} P_r^{-\frac{2}{3}} \left[1 + (Le - 1)\frac{h_D}{h_o} \right] \tag{31}$$

The total energy in dissociation in the free stream in BTU/lb weight of mixture, was evaluated approximately assuming that high-temperature air consists only of oxygen and nitrogen molecules and atoms, and that the dissociation of oxygen is complete before that of nitrogen begins. Then

$$h_D = D_o\,(Z - 1) \qquad (1 < Z < 1.211) \tag{32}$$

$$h_D = 0.211\,D_o + D_N\,(Z - 1.211) \quad (1.211 < Z < 2) \tag{33}$$

where the dissociation energy of oxygen and nitrogen, in BTU/lb weight of atomic products are $D_O = 7313$, $D_N = 14051$.

The compressibility of air is found from the curve fit formula $Z = f(p,\rho)$, equation (11). Curve fit formulas for the viscosity and Lewis number as functions of pressure and enthalpy, based on the data of reference (s), were employed. The Prandtl number was taken to be 0.72.

* In addition to the convective heat transfer there will be a contribution due to radiation from the hot gas. The radiative heat-transfer rate was computed in reference (q) and found to be small compared with the convective heat-transfer rate in the supersonic portion of the nozzle. For example, at supply conditions of 6000°K and 500 atmospheres, the radiative heat-transfer rate at the throat is about 400 BTU/ft^2, which is only one percent of the convective heat-transfer rate for these supply conditions. The radiative heat transfer will be neglected here.

RESULTS

A total of seven nozzles were designed by the method of characteristics with a turbulent boundary-layer correction. A block diagram of the computer programs used is shown in Figure 15. The design conditions and principal dimensions of the nozzles are given in Table I. The throat region is of particular interest because the convective heat-transfer rate is very much higher there than in other parts of the nozzle. Therefore, the boundary-layer growth and heat-transfer rate were computed in the throat region for 27 additional cases representing nozzles with a wide range of supply conditions and test-section Mach number. The results of the above calculations have made it possible to derive formulas, presented below, which correlate the peak throat heat-transfer rate and nozzle exit boundary-layer growth over a wide range of exit Mach number and supply conditions.

Nozzle Contours

The contours of a Mach 15 nozzle designed for true-temperature operation and a Mach 19 nozzle operating at the condensation-threshold are shown in Figure 16. The boundary-layer growth was computed using the Van Driest skin-friction law, based on the Prandtl mixing length hypothesis.

The isentropic contour of the Mach 15 nozzle is compared in Figure 17 with that of a perfect-gas nozzle (with $\gamma = 1.4$) having the same axial Mach number distribution and exit area. The difference between the contours is found to be rather small except in the throat region. This is due to the fact that at a relatively short distance downstream of the throat, the temperature has decreased to a value for which real-gas effects are small.

The effect of supply conditions on throat size is shown in Figure 18 where the dimensionless throat radius, r_*/r_e, is given for a nozzle with an exit Mach number of 11. The figure shows that the throat size decreases by an order of magnitude from the perfect-gas value as the supply temperature is increased to 10,000°K. Lowering the supply pressure results in a greater departure from a perfect gas at a given temperature, and further decrease the throat size. The throat size for a nozzle with a higher exit Mach number (and therefore lower exit temperature and pressure) may be found by multiplying the result from Figure 18 by the factor

$$F = \left[\left(\frac{A}{A_*}\right)_{M=11} \Big/ \left(\frac{A}{A_*}\right)_{M=M_E} \right]^{1/2} \qquad (34)$$

evaluated for a perfect gas. The results are presented for a Mach 11 nozzle (which will have essentially perfect-gas conditions at the exit for the range of supply conditions shown) in order to make it convenient to determine the throat size at higher Mach numbers using the same figure.

Boundary-Layer Growth and Heat Transfer

The heat-transfer rate and the growth of the boundary-layer total thickness δ, displacement thickness δ^*, and momentum thickness Θ, from the throat to the exit of the Mach 15 and 19 nozzles described in the preceding section, are shown in Figures 19 and 20. The boundary-layer growth and heat transfer in these two nozzles, as well as in the other nozzles which were designed, have the same general behavior. The acceleration of the air in the subsonic contraction thins the boundary layer and the convective heat-transfer rate rises rapidly. The boundary-layer thickness near the throat was found to be nearly independent of the initial value employed in starting the calculations at a low subsonic Mach number. A short distance upstream of the throat, the boundary-layer thickness has a minimum, and the heat transfer reaches its peak value.* A typical value of the boundary-layer thickness at the throat is a few thousandths of an inch, with the displacement thickness about one-tenth this value. The heat transfer here is of the order of thousands of BTU/ft^2sec. At the nozzle exit, the heat transfer has fallen by several orders of magnitude, to the order of one BTU/ft^2sec, while the boundary-layer thickness has increased by a very large factor, to a value of the order of several inches. The boundary layer grows

*As may be seen from equation (30), if the Stanton number and the recovery and wall enthalpies are constant, the maximum heat-transfer rate will occur at the throat, where $\rho_\infty u_\infty$ is a maximum. Due to the fact that St is decreasing as the throat is approached, the heat-transfer rate, which is nearly proportional to the product $\rho_\infty u_\infty$ St, has its maximum value upstream of the throat at a Mach number of about 0.85.

roughly linearly with distance from the throat. In view of these considerations, it is natural to divide the boundary-layer studies into two phases: the investigation of heat-transfer rates in the throat region; and the determination of the boundary-layer thickness at the nozzle exit.

a. Throat Heating

Exploratory throat heating calculations were first made to determine the effect of the subsonic inlet geometry. The dependence of the results on the skin-friction law employed was then investigated for a particular inlet. This was followed by calculations to determine the variation of throat heating with test-section Mach number and supply conditions for a selected inlet geometry and skin-friction law.

Figure 21 shows the heat-transfer distribution for three subsonic inlet geometries in a Mach 10.5 nozzle with a 2 ft^2 exit area operating at a supply pressure of 100 atm and a supply temperature of 5000°K. The Blasius incompressible skin-friction law (Appendix D, equation (D-1)) was employed with the heat transfer computed from Colburn's version of Reynolds analogy.

Two of the curves shown in Figure 21 are for a parabolic inlet as given by equation (19), with a throat radius of curvature R_c of 1 ft and 4 ft, respectively. The third curve is for a cubic inlet, described by equation (20), passing through a point $x_A = -0.5$ ft, $r_A = 0.5$ ft, with a radius of curvature of 4 ft at the throat. The calculations were carried a short distance downstream of the throat using an approximate supersonic contour, consisting of a parabola (having the same throat radius of curvature as the subsonic inlet) faired into a cone. The curves in Figure 21 also show that a larger throat radius of curvature results in high heat-transfer rates over a broader region upstream and downstream of the throat, but in a somewhat lower peak value. The two nozzle contours for R_c = 4 ft have the same supersonic geometry but different subsonic geometries. The merging of the corresponding heating curves downstream of the throat therefore indicates that the heat-transfer rate (and boundary-layer growth) along the supersonic contour is determined almost entirely by the local conditions, and is not appreciably influenced by the subsonic history of the boundary layer. This suggests the calculations to determine the boundary-layer correction for a nozzle could be satisfactorily initiated at the throat, with a small initial value of the momentum thickness.

Next, the effect on the heat-transfer rates resulting from the use of different skin-friction laws was investigated for the parabolic subsonic contour with $R_c = 4$ ft. The results are shown in Figure 22. The various skin-friction laws referred to in the figure are given in Appendices C and D. It can be seen that the peak heating rates vary all the way from 4200 BTU/ft^{2}sec for the Winkler formula to 12,300 BTU/ft^{2}sec for the Ludwieg-Tillman formula. The available measurements of turbulent heating in a partially dissociated boundary layer on a highly cooled surface (reference (r)) fall between these extremes. They agree best with the Blasius incompressible formula (Appendix D, equation (D-1)) used with Reynolds analogy as given in equation (31) with Le = 1.4. The experimental measurements referred to above were made on the cylindrical part of a hemisphere cylinder model mounted in a shock tube.

As shown in reference (t), the Blasius incompressible formula may be used to predict the skin friction on an adiabatic surface at hypersonic Mach numbers provided the density and viscosity are evaluated at a reference enthalpy as suggested by Eckert (reference (u)). However, when applied to a dissociated flow with a highly cooled wall, reference (r) indicates that the predicted heat-transfer rate is about 20 percent too high. It is interesting to note that the two versions of the Van Driest formula straddle the result given by the Blasius law with the reference enthalpy concept.

Figure 22 indicates that by far the greatest uncertainty in calculating throat heating lies in the choice of the skin-friction law. In subsequent heat-transfer calculations in the throat region, the Blasius incompressible law with the correction term for diffusion was employed, with the justification that this formula gives the best agreement with the available experimental results. The effect of including the term involving the Lewis number to allow for diffusion in the boundary layer is small.

Calculations were made of the boundary-layer growth and heat-transfer rate in the throat region of a family of 27 nozzles. The nozzles had an exit isentropic core area of 2 ft^2. The calculations were made for exit Mach numbers of 11, 15, and 19 with supply pressures of 50, 200, and 500 atmospheres, and supply temperatures of 2500°K, 5000°K, and 7500°K. The wall temperature was assumed to be 833°K (1500°R). A cubic subsonic contour, as given by equation (19), passing through the point (-0.5 ft, 0.5 ft) was used. The supersonic contour was approximated by a parabola faired into a cone. The radius of curvature, R_c, at the throat, was computed using the perfect-gas formula (Appendix B, equation (B-7)). Values of $(dM/dx^+)_{x^+ = 0}$ required in this formula were obtained from Figure 13; the throat radius r_* was determined from Figure 18.

The results for the supply temperature of 5000°K are shown in Figure 23. The appearance of the curves for supply temperatures of 2500°K and 7500°K are similar. In all cases the convective heat-transfer rate peaks a short distance upstream of the throat, at a Mach number of about 0.85. The heat-transfer rate falls to one-tenth of the peak value in a distance of a few inches on either side of the peak.

The peak heat-transfer rate is plotted versus supply pressure, with supply temperature as a parameter, in Figure 24. The peak heat-transfer rate which can be handled by convective water cooling of a copper nozzle is of the order of 10,000 BTU/ft^{2}sec. As may be seen from Figure 24, this rate is exceeded by several times at the higher supply temperatures and pressures.

In practical applications, the throat heating problem is greatly reduced by the very short running time provided in intermittent facilities such as a shock tunnel. For continuous operation, film cooling of the throat region appears to be one method which will permit nozzle operation at very high throat heat-transfer rates. Although the cooling effect on the wall vanishes a relatively short distance downstream of the injection point as the film absorbs heat, the region of high heat-transfer rates in the nozzle is also quite short. An analysis of the throat heating problem and its effect on the operating capabilities of a continuous, hypervelocity wind tunnel has been described in reference (q).

It was found that the peak heat-transfer rates could be correlated in terms of the four parameters p_o, T_o, r_*, and R_c. The results are well represented by the formula

$$\frac{q_H}{T_o - T_w} = 4.3\times10^{-3}\,\frac{p_o^{0.74}\,T_o^{0.31}}{(r_*\,R_c)^{0.05}} \qquad (35)$$

which is plotted in Figure 25. This formula contains the same parameters used by Sibulkin (reference (v)), who obtained an expression for the throat heat-transfer rate to a quadratic throat contour assuming an incompressible turbulent boundary layer with a near-adiabatic wall. The differences between the present formula for the heat-transfer coefficient and that of Sibulkin's can be traced to the fact that the present correlation was obtained for high-temperature air with a highly cooled wall and employed a cubic rather than a quadratic throat contour.

The values of Re_θ at the throat of the 27 nozzles for which heat-transfer calculations were made are plotted in Figure 26. It is seen that Re_θ falls in the range 430 to 16,000. These values are high enough so that turbulent flow might be expected in most cases, as stated earlier.

b. Boundary-Layer Growth

The boundary-layer growth was computed for the seven contoured nozzles listed in Table 1. The computations were started a short distance downstream of the throat, using as the initial momentum thickness the value obtained from the throat heating calculations. The Van Driest turbulent skin-friction formula with the Prandtl mixing length hypothesis was used (Appendix C, equation (C-9)). The Blasius incompressible skin-friction law used for the throat heating calculations is not suitable for the supersonic contour since such a formula does not take into account the decrease in friction coefficient with Mach number. Before the Van Driest formula was adopted, four preliminary runs were made in the first nozzle ($M_e = 11$, $p_o = 50$ atm, $T_o = 4000^\circ K$) comparing this formula with the Blasius formula modified by the reference enthalpy concept. The latter formula is known to accurately predict the skin-friction coefficient on an insulated flat plate in supersonic flow (see reference (t)). The results obtained with the two formulas at wall temperatures of $324^\circ K$ ($583^\circ R$) and $833^\circ K$ ($1500^\circ R$) are compared in Figure 27. The boundary-layer displacement thickness at the nozzle exit as obtained by the two methods differs only by four percent at the lower wall temperature, and by about 13 percent at the higher temperature. The use of some of the other friction laws given in Appendix C would lead to much larger differences in the boundary-layer thickness. The Van Driest formula was used in making final calculations of the boundary-layer growth in nozzles.

It was found possible to correlate the turbulent boundary-layer displacement thickness at the nozzle exit by a formula involving the nozzle exit Mach number M_e, the throat to exit length L, and supply conditions. The result is

$$\delta_e^* = 1.45 \times 10^{-6} \, T_o^{3/4} \, L^{4/5} \, M_e^{5/2} \, p_o^{-1/3} \tag{36}$$

δ_e^* will be given in feet when the temperature is in degrees Kelvin, the length in feet, and pressure in atmospheres. This correlation is plotted in Figure 28 for the seven nozzles listed in Table 1.

The variation of momentum thickness Reynolds number, Re_θ, in the Mach 15 and Mach 19 nozzles is shown in Figure 29. It is seen that Re_θ peaks a short distance downstream of the throat and decreases markedly towards the exit. The low value of Re_θ near the exit makes it necessary to examine the assumption made in the turbulent boundary-layer analysis that the laminar sublayer is thin. The laminar sublayer thickness in an incompressible flow may be computed from

$$\delta_\ell = C \nu_w / u_\tau \qquad (37)$$

where $u_\tau = (\tau_w/\rho_w)^{1/2}$ is the friction velocity and C is a constant. When this equation is applied to compressible flow, experimental results indicate that C varies from 11 at M = 8.3 to 14 at M = 10 (reference (w)). Using C = 14, the ratio of the laminar sublayer thickness to the total boundary-layer thickness at the nozzle exit was found to be 0.07 and 0.13 for the Mach number 15 and 19 nozzles, respectively. Therefore, the laminar sublayer is thin unless the value of C increases markedly at higher Mach numbers, or at very low Reynolds numbers.

At a sufficiently low value of Re_θ, reference (x) indicates that a turbulent boundary layer cannot exist. The minimum Reynolds number for turbulent flow given there is

$$Re_{\theta_{min}} = 43.6 \frac{\nu_{ref}}{\nu_\infty} \qquad (38)$$

This value of $Re_{\theta min}$ is 184 and 620 for the Mach 15 and 19 nozzles, respectively, as compared with nozzle exit value of 491 and 1811. Hence, reversion to laminar flow is not expected to occur.

Limitations of the Method

The design method that has been described is subject to a number of sources of error. Basically, the limiting assumption of equilibrium flow is an approximation for high-temperature air flows since at some point in the nozzle the gas will freeze into a mixture rich in atoms (see reference (d)). However, for sufficiently high nozzle supply densities the equilibrium assumption is a good one, because the amount of oxygen which freezes is very small, as shown in Figure 1.

The thermodynamic data for air (reference (m)) presently available involves significant error at the higher pressures due to the omission of a Van der Waals correction in the computation. Added to this is the error in the curve-fit formulas used to conveniently express the tabulated thermodynamic properties.

Insofar as the calculation of the boundary-layer growth and heat-transfer rates are concerned, the uncertainty in the skin-friction law far outweighs the sources of error inherent in the momentum integral method and in the use of Reynolds analogy. Also in the boundary-layer calculation, while the curve fits to the transport properties are accurate to within one percent, the transport coefficients were originally calculated in reference (s) by an approximate theory.

The computational procedure itself is only limited in accuracy by size of the discrete steps employed in the numerical procedure. Therefore, there is no inherent difficulty here.

In summary, besides the question of the validity of the equilibrium flow assumption, limitations are posed by the available data for the thermodynamic and transport properties of high-temperature air coupled with the lack of an appropriate skin-friction law. It is not possible to obtain a numerical estimate for the overall accuracy of the resultant nozzle contour at the present time.

CONCLUSIONS

A method has been described for designing axisymmetric nozzles for high-temperature equilibrium air with a turbulent boundary-layer correction. The assumption of equilibrium is approximately valid for many nozzle flows. The accuracy of the method is limited by the uncertainties in the data available for high-temperature air and in the friction law with a highly cooled wall.

For a given test-section size and Mach numbers the nozzle isentropic core contours were found to be quite similar to perfect-gas contours except in the vicinity of the throat, where the temperatures are high enough to cause large departures from the perfect-gas case. At elevated supply conditions, the throat size is an order of magnitude smaller than in a perfect-gas nozzle. Real-gas effects also result in a lower supply temperature and a much higher supply pressure than in a perfect-gas nozzle designed to achieve the same test-section conditions.

The calculations were made assuming a turbulent boundary layer. The boundary-layer momentum thickness Reynolds numbers were found to be high enough so that the assumption of a turbulent boundary layer is reasonable under most operating conditions.

The convective heat-transfer rate peaks a short distance ahead of the nozzle throat. The peak heat-transfer rate may be very large at elevated supply conditions; for example, it is of the order of 40,000 BTU/ft^2sec for a nozzle operating with supply conditions of 5000°K and 500 atm. The radiative heat-transfer rate to the nozzle throat is negligible compared with the convective flux, being of the order of one percent of the latter under the above conditions.

A comparison of the calculated convective turbulent heat-transfer rate in the throat region using various friction laws showed that the results obtained differ by as much as a factor of three between the laws at greatest variance with each other. The increase in heat transfer caused by diffusion of atoms in the boundary layer is difficult to predict accurately, but it is only of the order of ten percent. It was found that the peak throat heat-transfer rate could be correlated in terms of supply pressure, temperature, throat radius, and radius of curvature alone.

The boundary-layer thickness at the nozzle exit is also sensitive to the skin-friction law employed. The Van Driest formula, and the Blasius incompressible law evaluated at the reference enthalpy, gave results which differed by about three percent at a wall temperature of 324°K and 15 percent at 833°K for a typical nozzle. Since the boundary layer in hypervelocity nozzles is quite thick, the possible error in predicting the boundary-layer correction to the core co-ordinates may lead to a rather large departure from the desired exit Mach number. The nozzle exit displacement thickness as calculated using the Van Driest turbulent skin-friction law could be correlated for a wide range of conditions by a simple formula involving nozzle length, supply pressure, and temperature, and exit Mach number.

REFERENCES

(a) Thickstun, W. R., Schroth, R., and Lee, R., "The Development of an Axisymmetric Nozzle for Mach 8," Paper No. 34, Proceedings of the Fourth U. S. Navy Symposium on Aeroballistics, Dahlgren, Virginia, NAVORD Report 5904, 1 May 1958

(b) Persh, J. and Lee, R., "A Method for Calculating Turbulent Boundary Layer Development in Supersonic and Hypersonic Nozzles Including the Effects of Heat Transfer," NAVORD Report 4200, June 1956

(c) Moeckel, W. E. and Weston, K. C., "Composition and Thermodynamic Properties of Air in Chemical Equilibrium," NACA TN 4265, April 1958

(d) Glowacki, W. J., "Effect of Finite Oxygen Recombination Rate on the Flow Conditions in Hypersonic Nozzles," NOLTR 61-23 (to be published)

(e) Van Driest, E. R., "Calculation of the Stability of the Laminar Boundary Layer in a Compressible Fluid on a Flat Plate with Heat Transfer," JAS, Vol. 19, No. 12, pp. 801-812, December 1952

(f) Jack, J. R., Wisniewski, R. J., and Diaconis, N. S., "Effects of Extreme Surface Cooling on Boundary Layer Transition," NACA TN 4094, October 1957

(g) Stetson, K. F., "Boundary Layer Transition on Blunt Bodies with Highly Cooled Boundary Layers," IAS Report No. 59-36, presented at the 27th Annual Meeting, New York, 26-29 January 1959

(h) Korobkin, I. and Hastings, S. M., "Mollier Charts for Air in Dissociated Equilibrium at Temperatures of 2000°K to 15,000°K," NAVORD Report 4446, May 1957

(i) Wegener, P., Stollenwerk, E., Reed, S., and Lundquist, G., "NOL Hyperballistics Tunnel No. 4 Result I: Air Liquefaction," NAVORD Report 1742, January 1951

(j) Cronvich, L. L., "A Numerical Graphical Method of Characteristics for Axially Symmetric Isentropic Flow," JAS Vol. 15, No. 3, p. 155, March 1958

(k) Owen, J. M. and Sherman, F. S., "Design and Testing of a Mach 4 Axially Symmetric Nozzle for Rarefied Gas Flows," University of California Report No. HE-150-104, July 1952

(l) Grabau, M., "A Method of Forming Continuous Empirical Equations for the Thermodynamic Properties of Air From Ambient Temperatures to 15,000°K with Applications," AEDC TN 59-102, August 1959

(m) Hilsenrath, J. and Beckett, C. W., "Tables of Thermodynamic Properties of Argon-Free Air to 15,000°K," AEDC TN 52-12, September 1956

(n) Foelsch, K., "The Analytical Design of an Axially Symmetric Laval Nozzle for a Parallel and Uniform Jet," JAS, Vol. 16, No. 3, March 1949

(o) Persh, J., "A Theoretical Investigation of Turbulent Boundary Layer Flow with Heat Transfer at Supersonic and Hypersonic Speeds," NAVORD Report 3854, May 1955

(p) Winkler, E. M. and Cha, M. H., "Investigation of Flat Plate Hypersonic, Turbulent Boundary Layers with Heat Transfer at a Mach Number of 5.2," NAVORD Report 6631, September 1959

(q) Enkenhus, K. R., Harris, E. L., Glowacki, W. J., Maher, E. F., and Ceretta, P. A., "The Simulation of Re-entry Conditions in the Wind Tunnel," paper presented at the Institute of Environmental Sciences Meeting, Washington, D. C., 9 April 1961

(r) Rose, P. H., Probstein, R. F., and Adams, M. C., "Turbulent Heat Transfer Through a Highly Cooled Partially Dissociated Boundary Layer," AVCO Research Report No. 14, January 1958

(s) Hansen, C. F., "Approximations for the Thermodynamic and Transport Properties of High Temperature Air," NACA TN 4150, March 1958

(t) Hayes, W. D. and Probstein, R. F., "Hypersonic Flow Theory," Academic Press, New York, p. 329, 1959

(u) Eckert, E. R. G., "Engineering Relations for Friction and Heat Transfer to Surfaces in High Velocity Flow," JAS, Vol. 22, pp. 585-587, 1955

(v) Sibulkin, M., "Heat Transfer to an Incompressible Turbulent Boundary Layer and Estimation of Heat-Transfer Coefficients at Supersonic Nozzle Throats," JPL Report 20-78, July 1954

(w) Hill, F. K., "Turbulent Boundary Layer Measurements at Mach Numbers from 8 to 10," Physics of Fluids, Vol. 2, No. 6, pp. 668-680, November-December 1959

(x) Tetervin, N., "An Estimate of the Minimum Reynolds Number for Transition from Laminar to Turbulent Boundary-Layer Flow by Means of Energy Considerations," NAVORD Report 6854, November 1960

(y) Enkenhus, K. R. and Tucker, N. B., Design and Testing of an Axisymmetric Flow Nozzle for Mach Number 7," UTIA Technical Note No. 4, January 1955

(z) Van Driest, E. R., "Turbulent Boundary Layer in Compressible Fluids," JAS, March 1951

(aa) Hidalgo, H., "On the Application of Van Driest's Method to a Highly Cooled, Partially Dissociated Turbulent Boundary Layer," Jet Propulsion, Vol. 28, No. 7, pp. 487-489, July 1958

(bb) Reshotko, E. and Tucker, M., "Approximate Calculation of the Compressible Turbulent Boundary Layer with Heat Transfer and Arbitrary Pressure Gradient," NACA TN 4154, December 1957

APPENDIX A

Determination of Basic Nozzle Geometry

The basic geometry of an axisymmetric perfect-gas Foelsch nozzle is shown in Figure 30. Radial source flow is assumed to exist in the region BCD, bounded by the Mach lines BC and CD through the inflection point C. The apparent source of the radial flow is at 0. The test-section Mach number is reached at D, so that x_t equals AD. The tangent of the maximum half-expansion angle ω is equal to the slope at C. The Mach number is assumed to vary linearly along AB, from the throat to the beginning of the radial flow region, with a gradient equal to $(dM/dx)_B$.

For radial flow through a spherical cap a distance y from the source (point 0) the one-dimensional relationship between area ratio and Mach number is valid. Therefore

$$y/y_* = \left[\frac{A}{A_*}(M)\right]^{\frac{1}{2}} = \left(\frac{1}{M}\left\{\frac{2}{\gamma+1}\left[1+\frac{\gamma-1}{2}M^2\right]\right\}^{\frac{\gamma+1}{2(\gamma-1)}}\right)^{\frac{1}{2}} \qquad \text{(A-1)}$$

where y_* is the radial distance at which sonic velocity would exist. A second property of source flow is that along a Mach line (such as BC or CD, Figure 30) the change in flow direction necessary to produce a given change in Mach number from the value one is exactly half the Prandtl-Meyer angle $Ⓗ(M)$ tabulated for two-dimensional flow (reference (n)). From these properties, the following relations may be derived for the nozzle geometry shown in Figure 30 (see reference (y) for details):

$$Ⓗ(M_c) = Ⓗ(M_e) - 2\omega \qquad \text{(A-2)}$$

$$Ⓗ(M_B) = Ⓗ(M_e) - 4\omega \qquad \text{(A-3)}$$

$$\left(\frac{dM}{dx^+}\right)_{x^+=0} = \left(\frac{dM}{dx^+}\right)_B = \frac{2M_B}{5y_*^+(M_B^2-1)}\left(\frac{6M_B}{5+M_B^2}\right)^{\frac{1}{2}} \qquad \text{(A-4)}$$

where

$$y_*^+ = 1\Big/\left(2\sin\left(\frac{\omega}{2}\right)\left[\frac{A}{A_*}(M_B)\right]^{\frac{1}{2}}\right). \qquad \text{(A-5)}$$

The dimensionless distance to the beginning of the test cone may be found by summing components as follows:

$$x_t^+ = \underbrace{\frac{M_B - 1}{(dM/dx^+)_B}}_{AB/r_e} + \underbrace{(y_{C'}^+ \cos\omega - y_B^+)}_{BC'/r_e} + \underbrace{(y_D^+ - y_{C'}^+ \cos\omega)}_{C'D/r_e} \tag{A-6}$$

$$= \frac{M_B - 1}{(dM/dx^+)_B} - y_B^+ + y_D^+$$

The overall length of the nozzle is

$$L^+ = x_t^+ + \cot\bar{\mu}_e \; . \tag{A-7}$$

By means of equations (A-1) through (A-6), the parameters x_t^+ and $(dM/dx^+)_{x^+ = 0}$ needed to determine the Mach number distribution may be found by prescribing the desired exit Mach number M_e and a suitable maximum angle ω for the contour.

APPENDIX B

Throat Radius of Curvature

By definition, the radius of curvature of the throat is

$$R_c = \left[1 + (dr/dx)^2_{x=0}\right]^{3/2} \Big/ \left(\frac{d^2r}{dx^2}\right)_{x=0} . \qquad \text{(B-1)}$$

Noting that $(dr/dx)_{x=0} = 0$ and rewriting equation (B-1) in terms of the area $A = \pi r^2$, the expression for R_c becomes

$$R_c = 2\pi r_* \Big/ \left(\frac{d^2A}{dx^2}\right)_{x=0} . \qquad \text{(B-2)}$$

Assume the existence of the two functions

$$M = M(x) \qquad \text{(B-3)}$$

$$A/A_* = f(M) \qquad \text{(B-4)}$$

where A/A_* is the one-dimensional area ratio. Now, rewriting equation (B-2) in terms of these functions, and noting that

$$\left[\frac{d(A/A_*)}{dM}\right]_{x=0} = 0$$

i.e., the area passes through a minimum, there results the desired expression for R_c:

$$R_c = 2 \Big/ \left(r_* \cdot \left[\frac{d^2(A/A_*)}{dM^2}\right]_{x=0} \cdot \left(\frac{dM}{dx}\right)^2_{x=0} \right) . \qquad \text{(B-5)}$$

The throat height r_* is known by computation. Equation (B-3) is provided by the prescribed axial Mach number distribution. Therefore, only equation (B-4) need be supplied for computation of R_c by equation (B-5).

a. Perfect-Gas Case

Equation (B-4) is given by

$$\frac{A}{A_*} = \frac{1}{M}\left\{\frac{2}{\gamma+1}\left(1+\frac{\gamma-1}{2}M^2\right)\right\}^{\frac{\gamma+1}{2(\gamma-1)}} \qquad \text{(B-6)}$$

Therefore, R_c is easily computed by equation (B-5) and is

$$R_c = \frac{\gamma+1}{2r_*\left(\frac{dM}{dx}\right)^2_{x=0}} \qquad \text{(B-7)}$$

b. Real-Gas Case

There is no analytical expression for equation (B-4) in this case. However, an approximate expression can be formed by fitting a curve to the area-ratio values tabulated in the isentropic expansion tables as a function of Mach number. This need only be done in the region near Mach number one. The fit $A/A_*(M)$ obtained may be used to evaluate R_c by means of equation (B-5). Of course, the accuracy of the second derivative of any curve fit may be poor. Therefore, the resultant value of R_c obtained by this method must be treated with reservation.

APPENDIX C

Extension of the Van Driest Turbulent Skin-Friction Formula to Calculations in Dissociated Flows with Pressure Gradient

This appendix presents the derivation of an expression for applying the Van Driest turbulent skin-friction formula to dissociated flows with pressure gradient. The fundamental assumption is that the local skin friction on a curved body is the same as that on a flat plate having the same local external flow conditions and value of Re_θ.

The Van Driest formula (see reference (z)) was derived for a turbulent boundary layer in a compressible fluid with zero pressure gradient. This formula was revised for application to a highly cooled, partially dissociated boundary layer by H. Hidalgo (reference (aa)). Hidalgo has shown that, under certain assumptions, the Van Driest relation may be applied to a dissociated flow merely by replacing the temperature in the formula by the corresponding value of the enthalpy. These assumptions are:

a. The turbulent and laminar Lewis numbers are unity.

b. The turbulent and laminar Prandtl numbers are unity.

c. The density fluctuations in the boundary layer are negligible.

d. The product of density and enthalpy is constant across the boundary layer. (This statement is essentially true except in a thin region near the wall.) The skin-friction formula obtained is then

$$\frac{0.242}{B\, C_f^{1/2}\left(\frac{h_w}{h_e}\right)^{1/2}}\left(\sin^{-1}\alpha + \sin^{-1}\beta\right) = 0.41 + \log_{10}\left[R_{e_x} C_f \frac{\mu_e}{\mu_w} DE\right] \qquad \text{(C-1)}$$

where

$$B^2 = \frac{u_e^2/2h_e}{h_w/h_e} \qquad C = \frac{h_o/h_e}{h_w/h_e} - 1$$

$$\alpha = \frac{2B^2 - C}{\left(C^2 + 4B^2\right)^{\frac{1}{2}}} \qquad \beta = \frac{C}{\left(C^2 + 4B^2\right)^{1/2}}$$

$$D = \frac{\rho_\infty h_\infty}{\rho_w h_w}$$

$$E = \left(h_w/h_\infty\right)^{-\frac{1}{2}} \qquad \text{(assumes Prandtl mixing length)}$$

or

$$E = 1 \qquad \text{(assumes von Karman similarity)}$$

In making computations on blunt bodies, or where a pressure gradient exists, the flat-plate formula cannot be directly applied; however, the boundary-layer growth can be computed using the momentum integral equation in which the skin friction is expressed as a function of Re_θ. The Van Driest skin-friction formula may be expressed in terms of Re_θ rather than Re_x (where x is the distance from the leading edge of the plate) by making use of the relation

$$\frac{d(Re_\theta)}{d(Re_x)} = \frac{d\theta}{dx} = C_f/2 .$$

Thus,

$$Re_\theta = \int_0^x \frac{C_f}{2}\, d(Re_x) \qquad \text{(C-2)}$$

For any position on the surface, a value of C_f will then be uniquely determined by the values of u_∞, h_∞, h_w, p_∞, and Re_θ.

For brevity, equation (C-1) may be written as:

$$C_1/\sqrt{C_f} = C_2 + \log_{10}\left(C_3\, C_f\, Re_x\right) \qquad \text{(C-3)}$$

where

$$C_1 = \frac{0.242}{u_\infty}\left(\sin^{-1}\alpha + \sin^{-1}\beta\right)\left(2h_\infty\right)^{\frac{1}{2}}$$

$$C_2 = 0.41 \qquad C_3 = \frac{\mu_\infty}{\mu_w} D E$$

It is noted in reference (aa) that C_2 is a weak function of D; $0.41 \leq C_2 \leq 0.45$ for $1.0 \leq D \leq 2.5$; thus, a more nearly correct value of C_2 would be:

$$C_2 = 0.41 + 0.027(D-1) \quad .$$

Now, solving equation (C-3) for Re_x in terms of C_f letting $t = 1/(C_f)^{1/2}$

$$Re_x = G t^2 e^{Ht} \tag{C-4}$$

where

$$G = \frac{1}{C_3} e^{-2.303 C_2} \tag{C-5a}$$

and

$$H = 2.303 C_1 \quad . \tag{C-5b}$$

Differentiating:

$$d(Re_x) = G\left(2t e^{Ht} + H t^2 e^{Ht}\right) dt \quad . \tag{C-6}$$

Inserting this in equation (C-2) and integrating from a point near (but not at) the leading edge where $C_f = C_{f_0}$ and $Re_\theta = Re_{\theta_0}$ there results,

$$Re_\theta - Re_{\theta_0} = \int_{Re_{x_0}}^{Re_x} \frac{d(Re_x)}{2t^2} = \int_{t_0}^{t} G\left(\frac{H e^{Ht}}{2} + \frac{e^{Ht}}{t}\right) dt = f(t) - f(t_0) \tag{C-7}$$

where

$$f(t) = G\left[\frac{1}{2} e^{Ht} + \ln t + \sum_{n=1}^{\infty} \frac{H^n t^n}{n\, n!}\right] \quad . \tag{C-8}$$

From equation (C-3), $C_f \to \infty$ as $Re_x \to 0$, so that $t_o \to 0$ at the leading edge. The nature of the Van Driest friction formula leads to a singularity at the leading edge, i.e.,

$$\lim_{t_o \to 0} f(t_o) = -\infty \quad .$$

If, however, the integration is begun a short distance from the leading edge where $Re_{\theta_o} \ll Re_\theta$, it can be shown that $f(t_o) \ll f(t)$. On this basis, we obtain

$$Re_\theta = G\left[\frac{e^{H \cdot C_f^{-1/2}}}{2} + \ln t + \sum_{n=1}^{\infty} \frac{H^n C_f^{-n/2}}{n \cdot n!}\right] \quad . \qquad \text{(C-9)}$$

Equation (C-9) is the desired final relationship between C_f and Re_θ. It is an implicit formula and is solved for C_f by an iterative scheme, based on an initial guess for C_f obtained from some other turbulent skin-friction formula.

APPENDIX D

Empirical Skin-friction Laws

Other turbulent friction formulas from which calculations were made were the following:

a. The Blasius incompressible skin-friction law, used for the majority of the throat heating calculations, is

$$C_f = 0.0246\left(\frac{\rho_\infty u_\infty \theta}{\mu_\infty}\right)^{-\frac{1}{4}} \quad \text{(D-1)}$$

The constant is chosen to agree with the experimental results for incompressible flow as compiled by Winkler and Cha (reference (p)).

b. The Blasius incompressible law, with values of viscosity and density corresponding to a reference enthalpy, as proposed by Eckert (reference (u)). This law is

$$C_f = 0.0246\left(\frac{\rho_{ref} u_\infty \theta}{\mu_{ref}}\right)^{-\frac{1}{4}}\left(\frac{\rho_{ref}}{\rho_\infty}\right)^{5/4} \quad \text{(D-2)}$$

The reference enthalpy is

$$h_{ref} = \frac{1}{2}\left(h_w + h_\infty\right) + 0.22\left(h_{ad} - h_\infty\right) \quad \text{(D-3)}$$

where h_{ad} is given by equation (27a).

c. The Ludwieg-Tillman skin-friction law, modified to include the reference enthalpy concept (reference (bb))

$$C_f = 0.246\, e^{-1.561\left(\delta^*/\theta\right)_i}\left(\frac{\rho_{ref} u_\infty \theta}{\mu_{ref}}\right)^{-0.268}\left(\frac{\rho_{ref}}{\rho_\infty}\right)^{1.268} \quad \text{(D-4)}$$

The exponential term allows for the effect of a local pressure gradient on skin friction through the incompressible form factor $(\delta^*/\theta)_i$, given by

$$\left(\delta^*/\theta\right)_i = \left(\frac{\delta^*}{\theta}+1\right)\frac{h_\infty}{h_e} - \left(\frac{h_w}{h_e}-1\right)\left(\frac{\delta^*}{\theta}\right)_{\infty,fp} \quad \text{(D-5)}$$

where $(\delta^*/\theta)_{i,fp}$ is the incompressible form factor on a flat plate, which may be taken equal to 1.286. This equation is given in reference (bb) in terms of temperature ratios; it is assumed that for high temperatures the corresponding enthalpy ratios may be used.

d. The Winkler skin-friction formula

$$C_f = 0.0246\left(\frac{\rho_\infty u_\infty \theta}{\mu_\infty}\right)^{-\frac{1}{4}} \cdot \left(\frac{h_e}{h_w}\right)^{\frac{1}{2}} \cdot \left(\frac{h_w}{h_{ad}}\right)^{\frac{1}{4}} \qquad (1\text{-}6)$$

This empirical formula (in which the corresponding enthalpy ratios have been substituted for the temperature ratios of the original formula) was derived from an examination of a large amount of compressible turbulent skin-friction data with cooled walls; it is valid for low air temperatures (reference (p)).

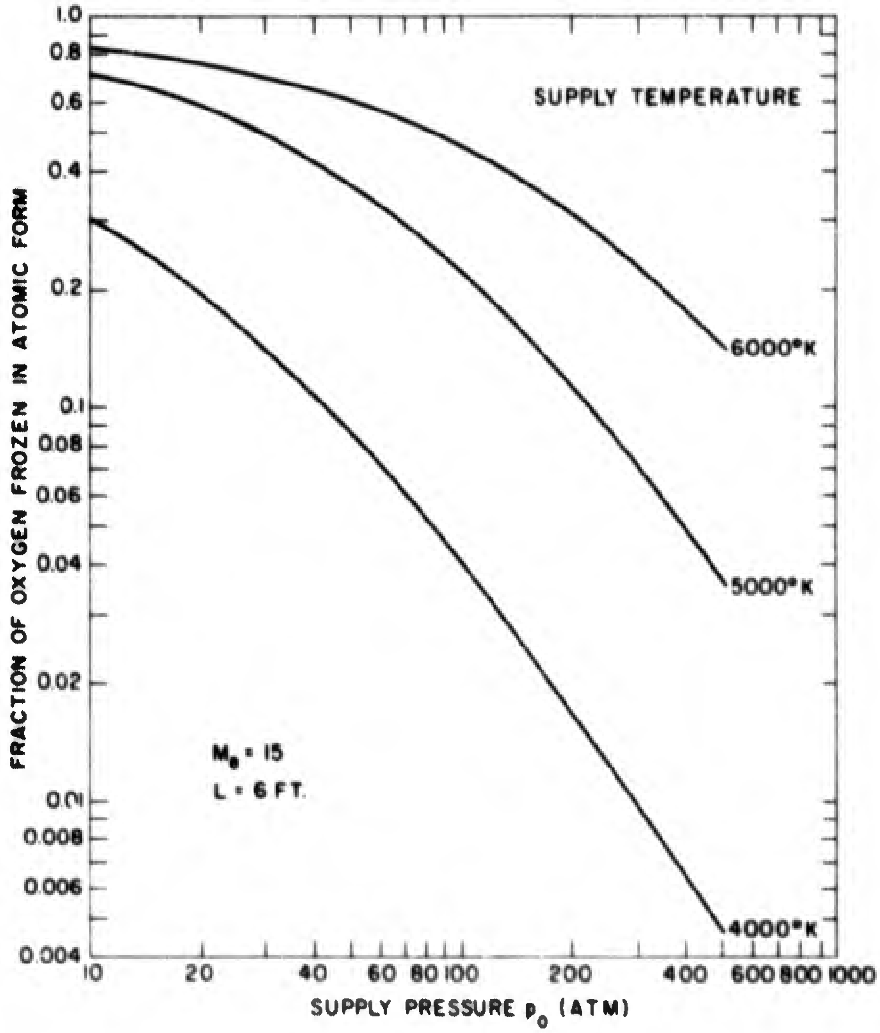

FIG I FRACTION OF OXYGEN FROZEN IN ATOMIC FORM IN A CONICAL NOZZLE

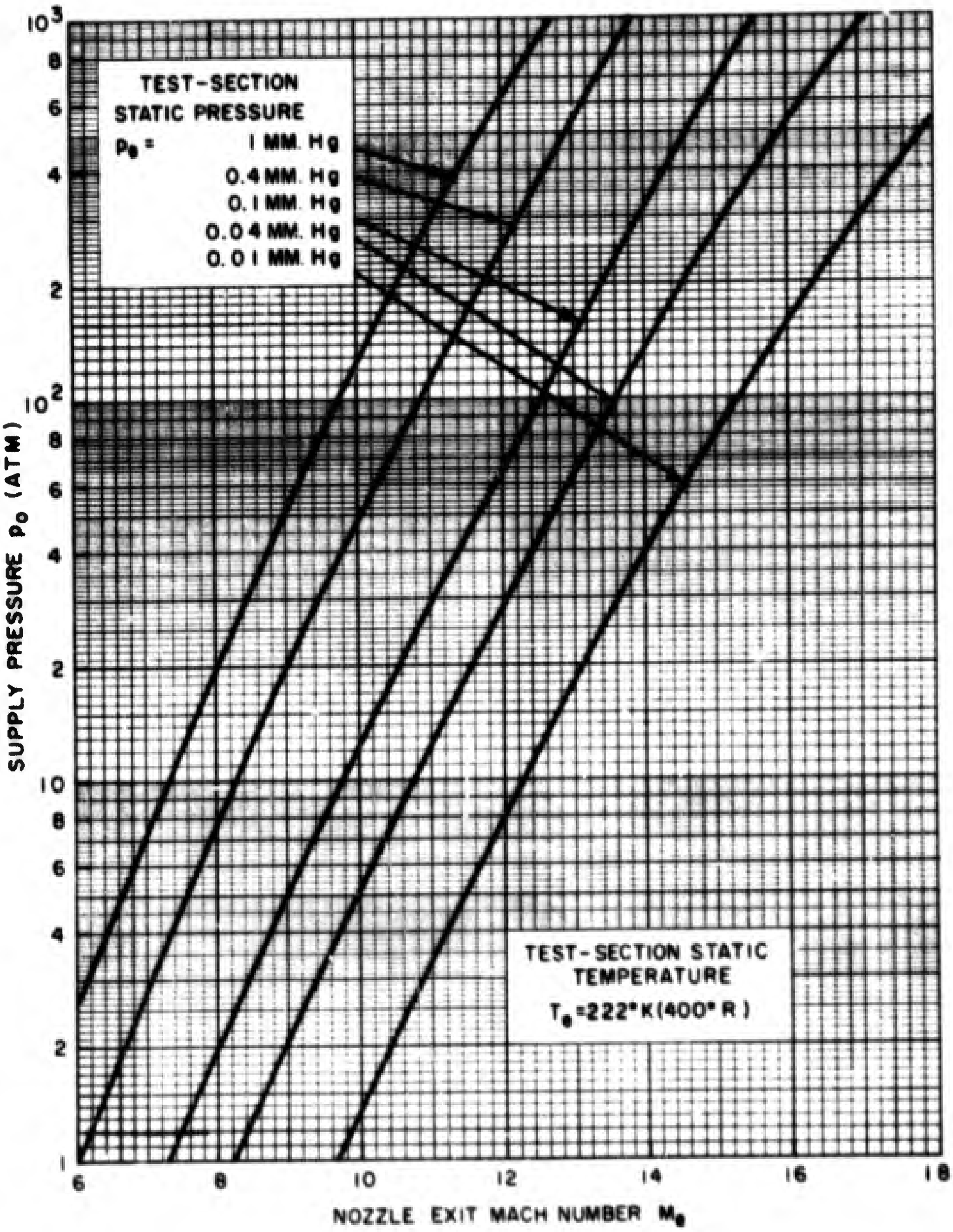

FIG. 2 SUPPLY PRESSURE REQUIRED FOR TRUE-TEMPERATURE OPERATION

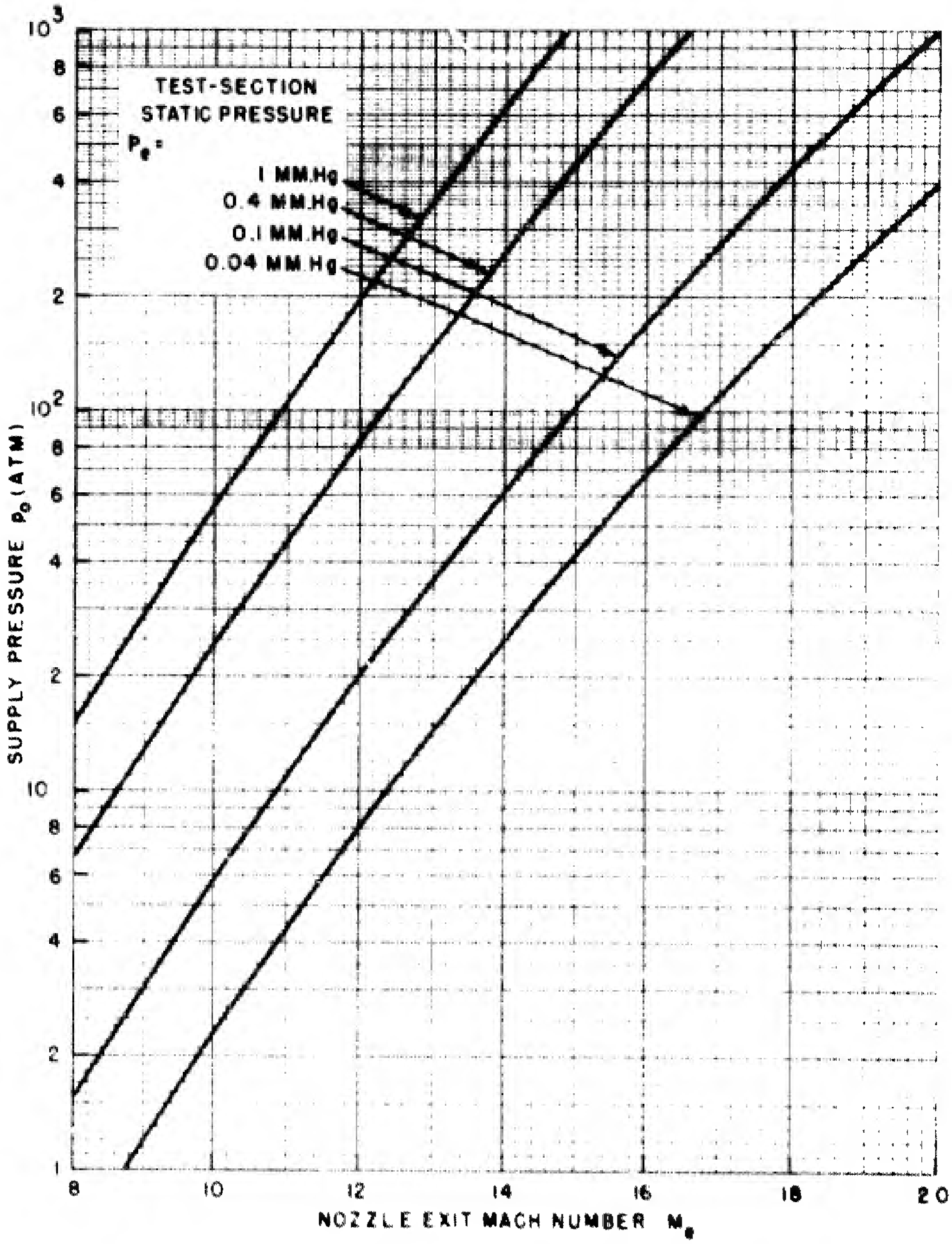

FIG. 3 SUPPLY PRESSURE REQUIRED FOR CONDENSATION-THRESHOLD OPERATION

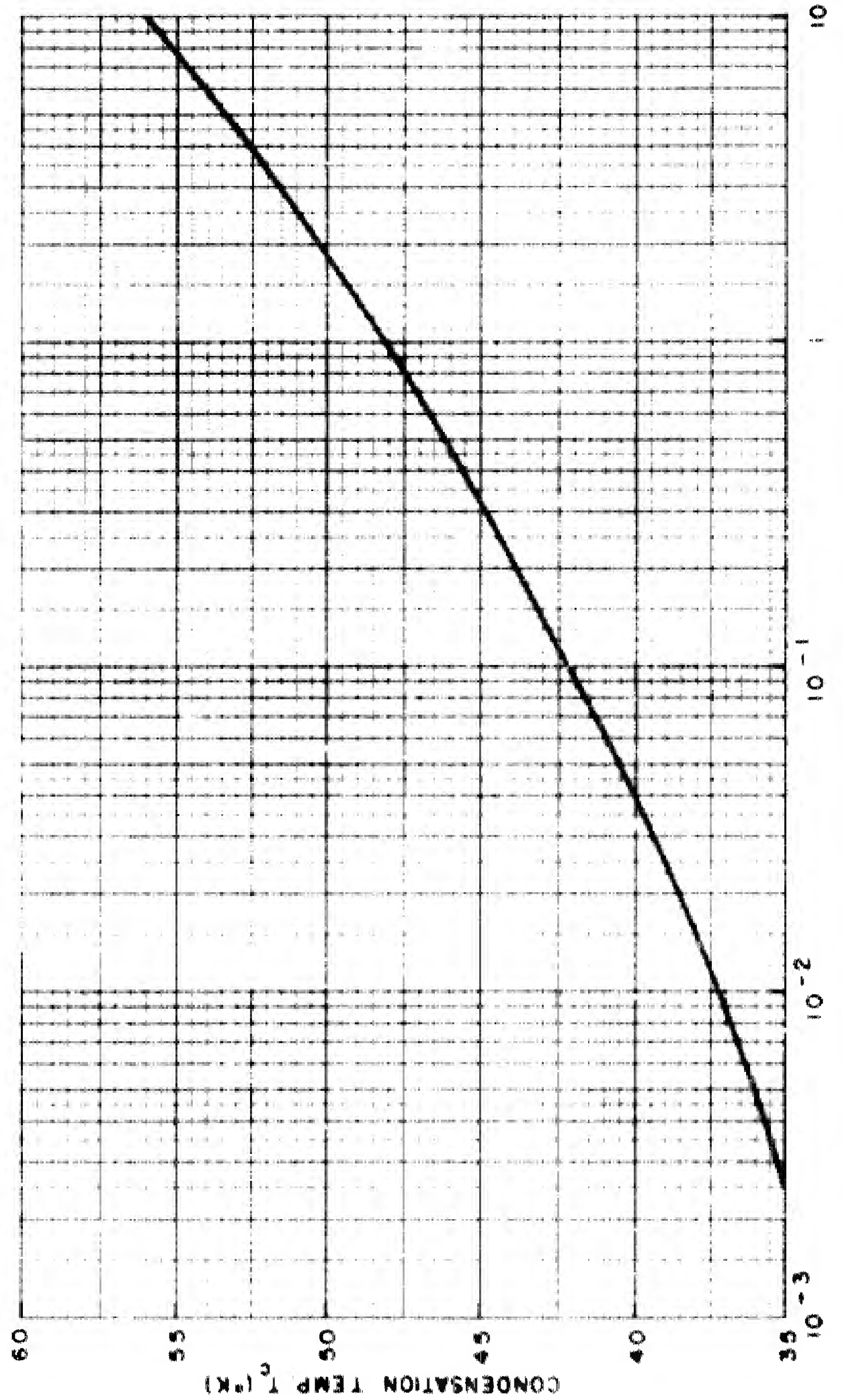

FIG. 4 AIR CONDENSATION TEMPERATURE

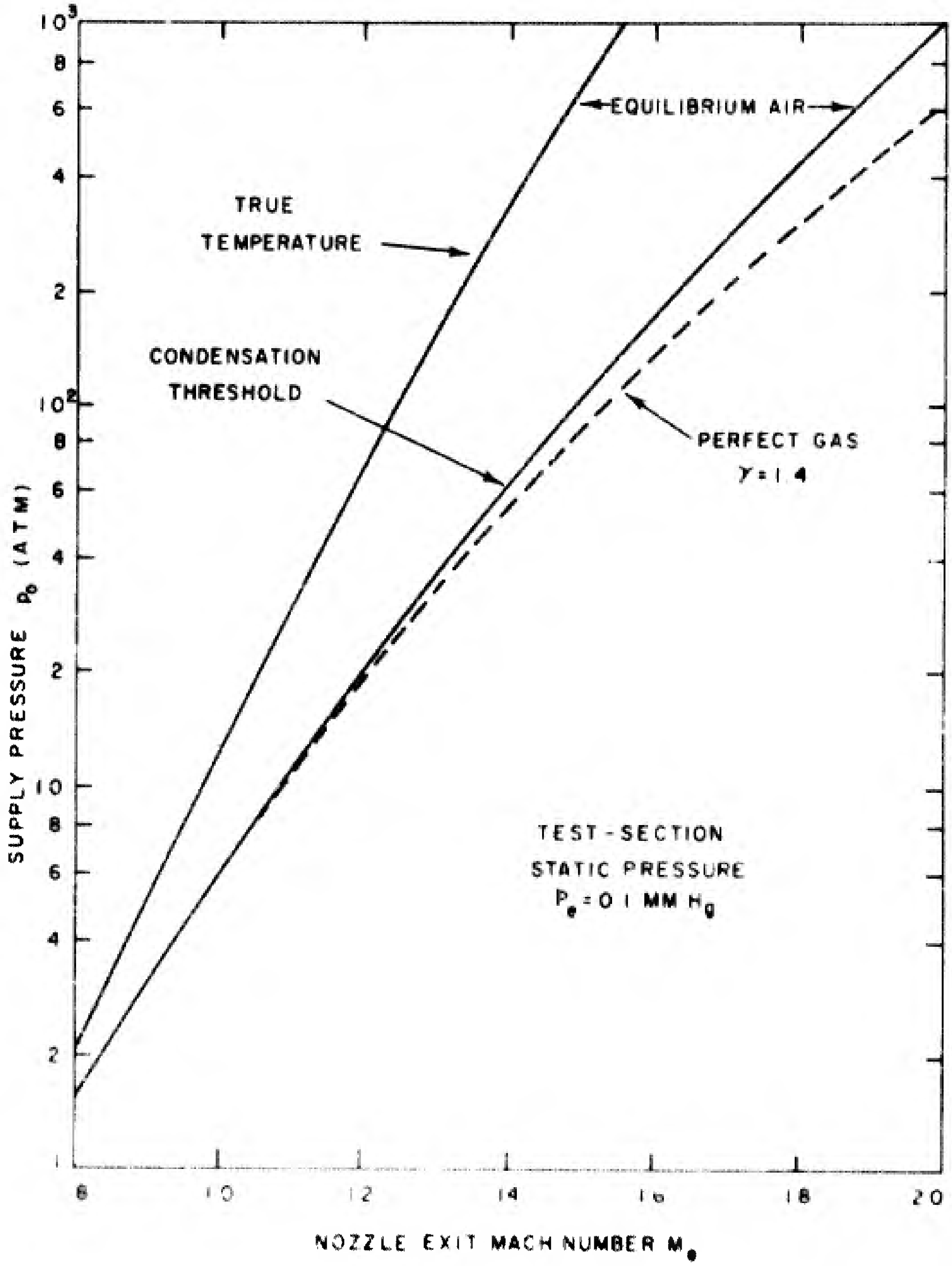

FIG. 5 COMPARISON OF SUPPLY PRESSURE REQUIREMENTS

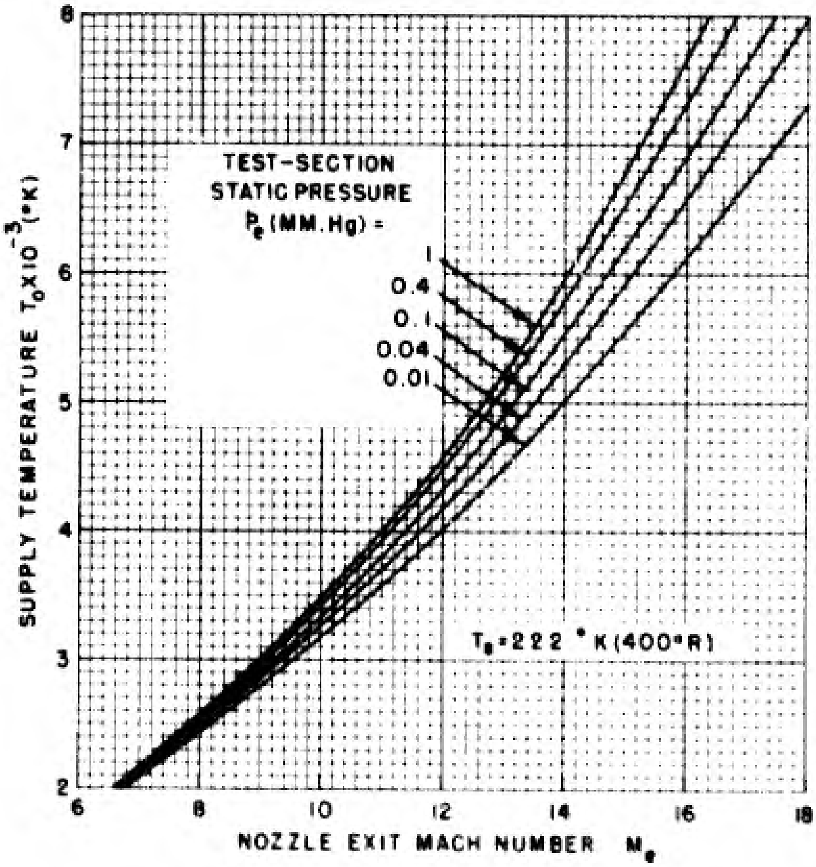

FIG. 6 SUPPLY TEMPERATURE REQUIRED
FOR TRUE-TEMPERATURE OPERATION

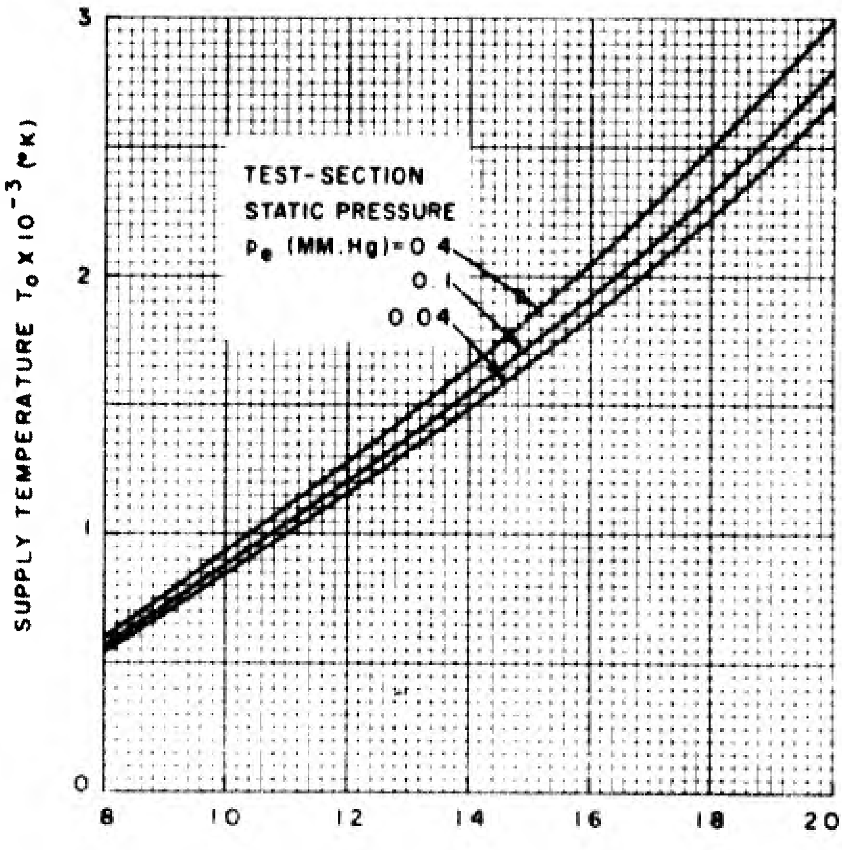

FIG 7 SUPPLY TEMPERATURE REQUIRED FOR CONDENSATION – THRESHOLD OPERATION

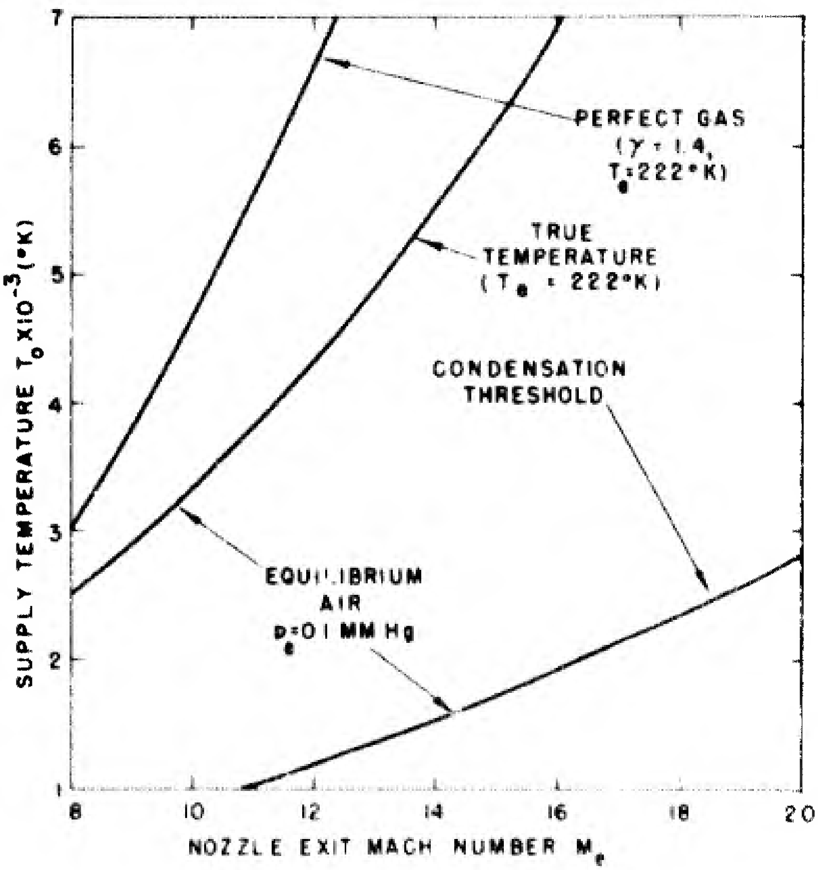

FIG. 8 COMPARISON OF SUPPLY TEMPERATURE REQUIREMENTS

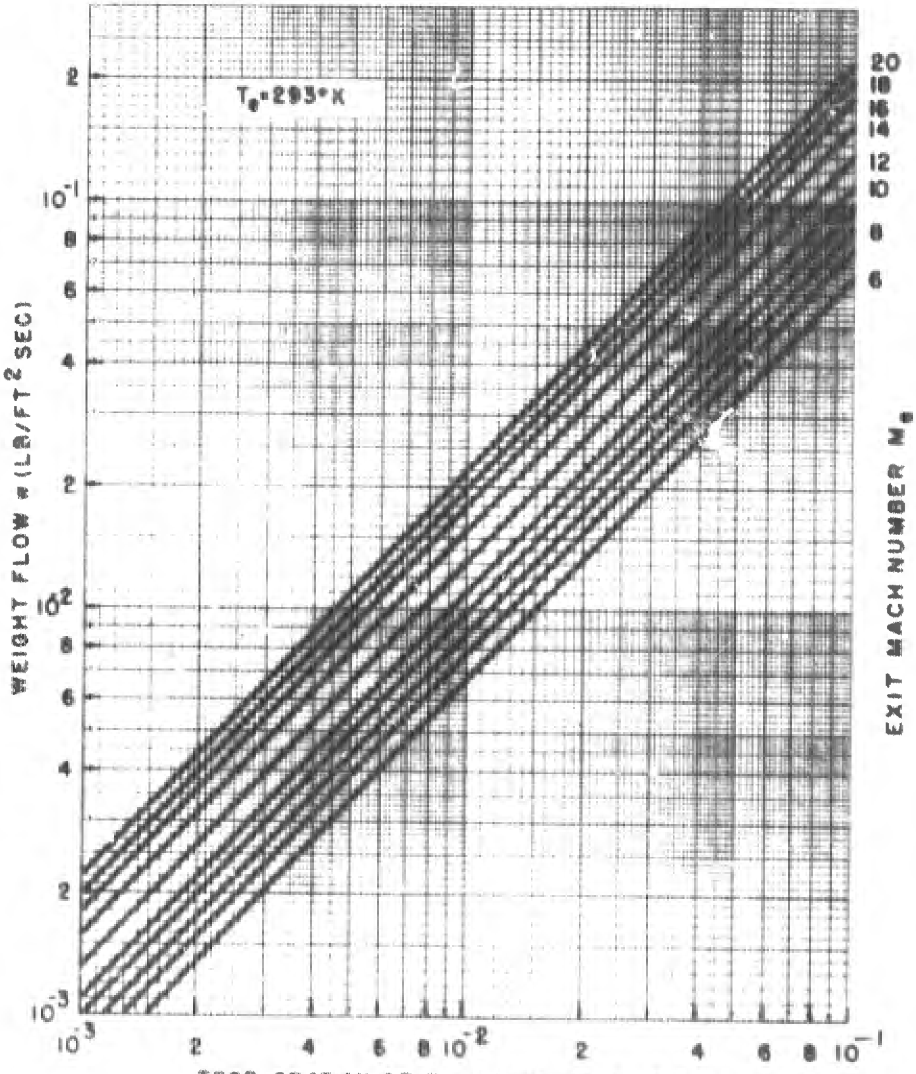

FIG 9a WEIGHT FLOW PER UNIT EXIT AREA

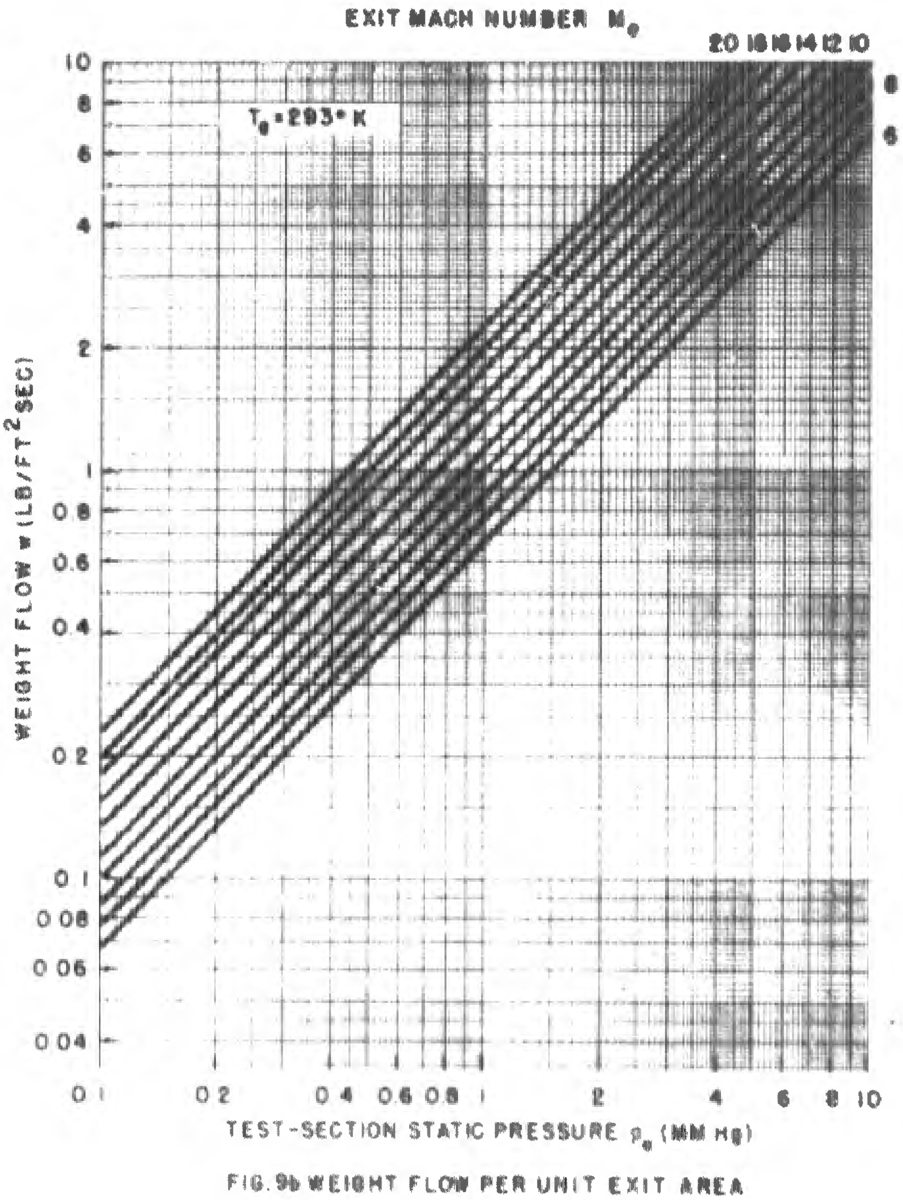

FIG. 9b WEIGHT FLOW PER UNIT EXIT AREA

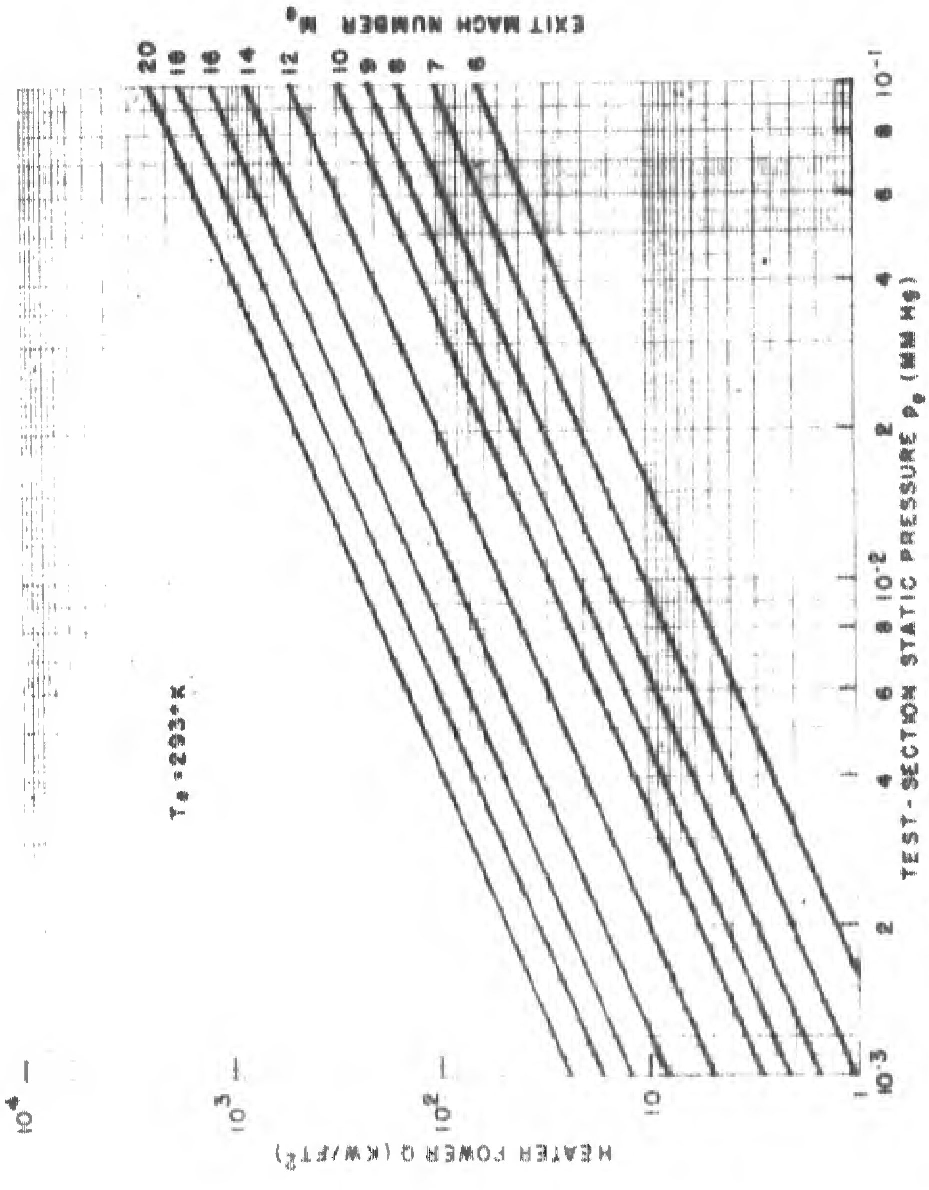

FIG. 10a AIR HEATING POWER PER UNIT EXIT AREA

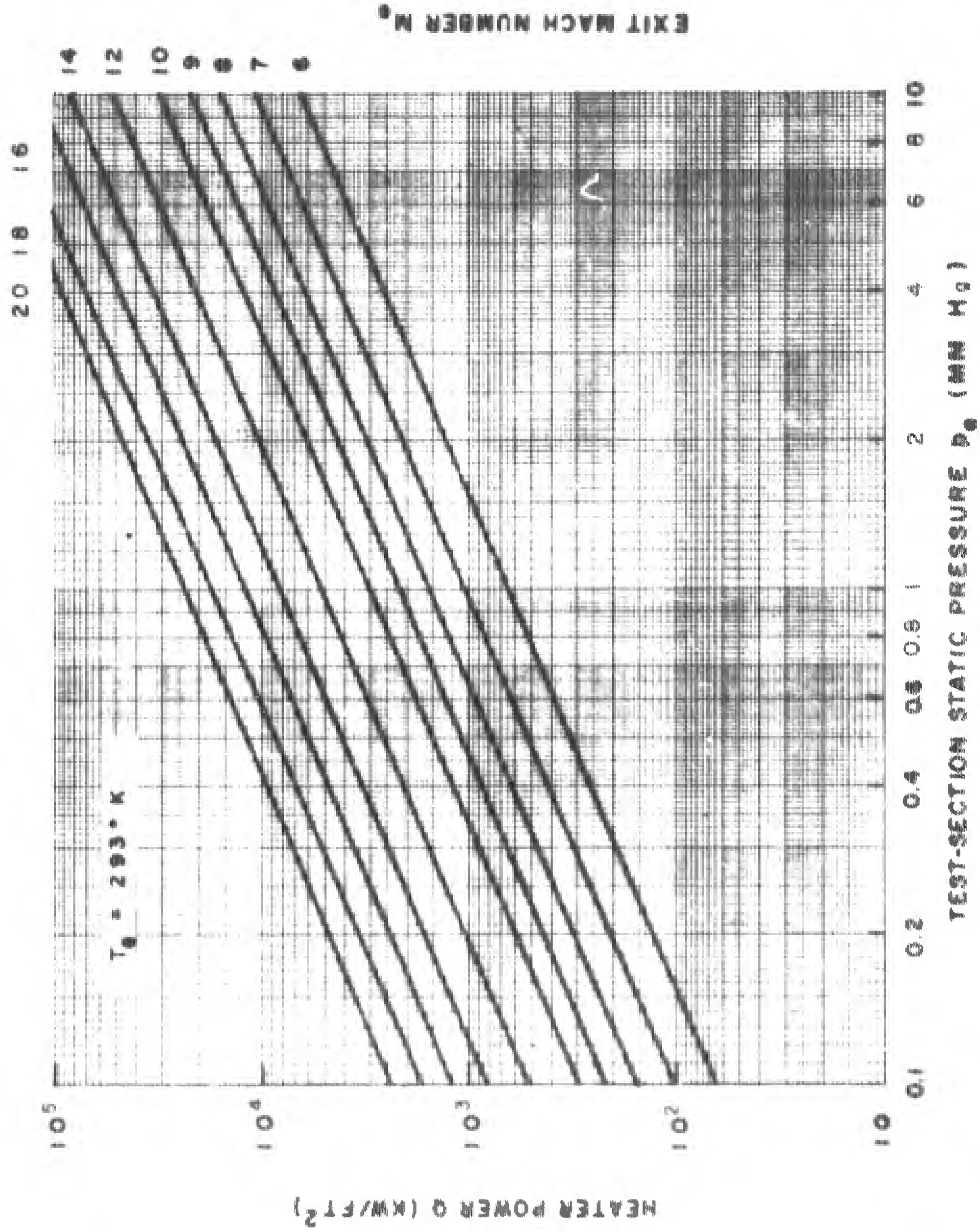

FIG. 10b AIR HEATING POWER PER UNIT EXIT AREA

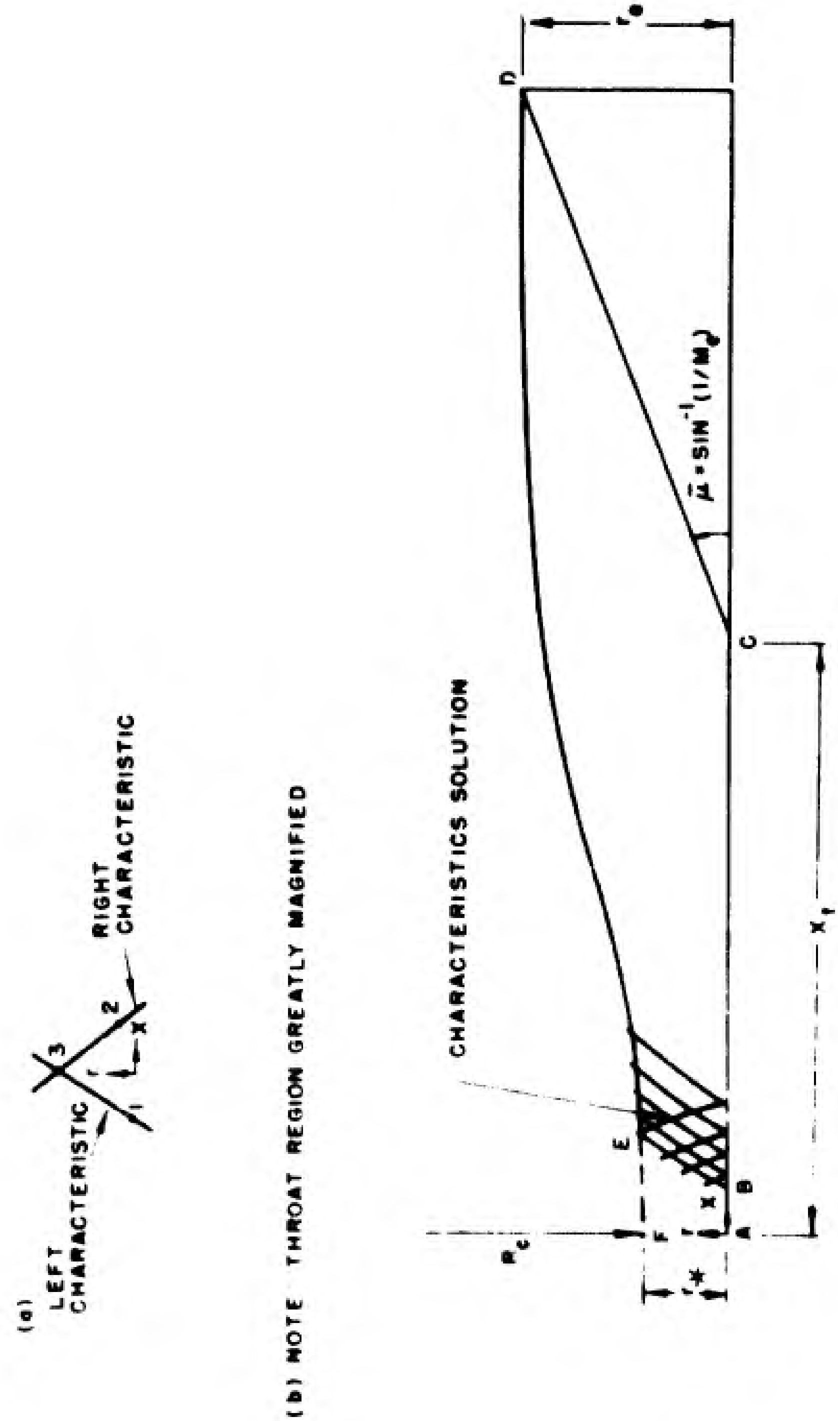

FIG. 11 CHARACTERISTIC NET

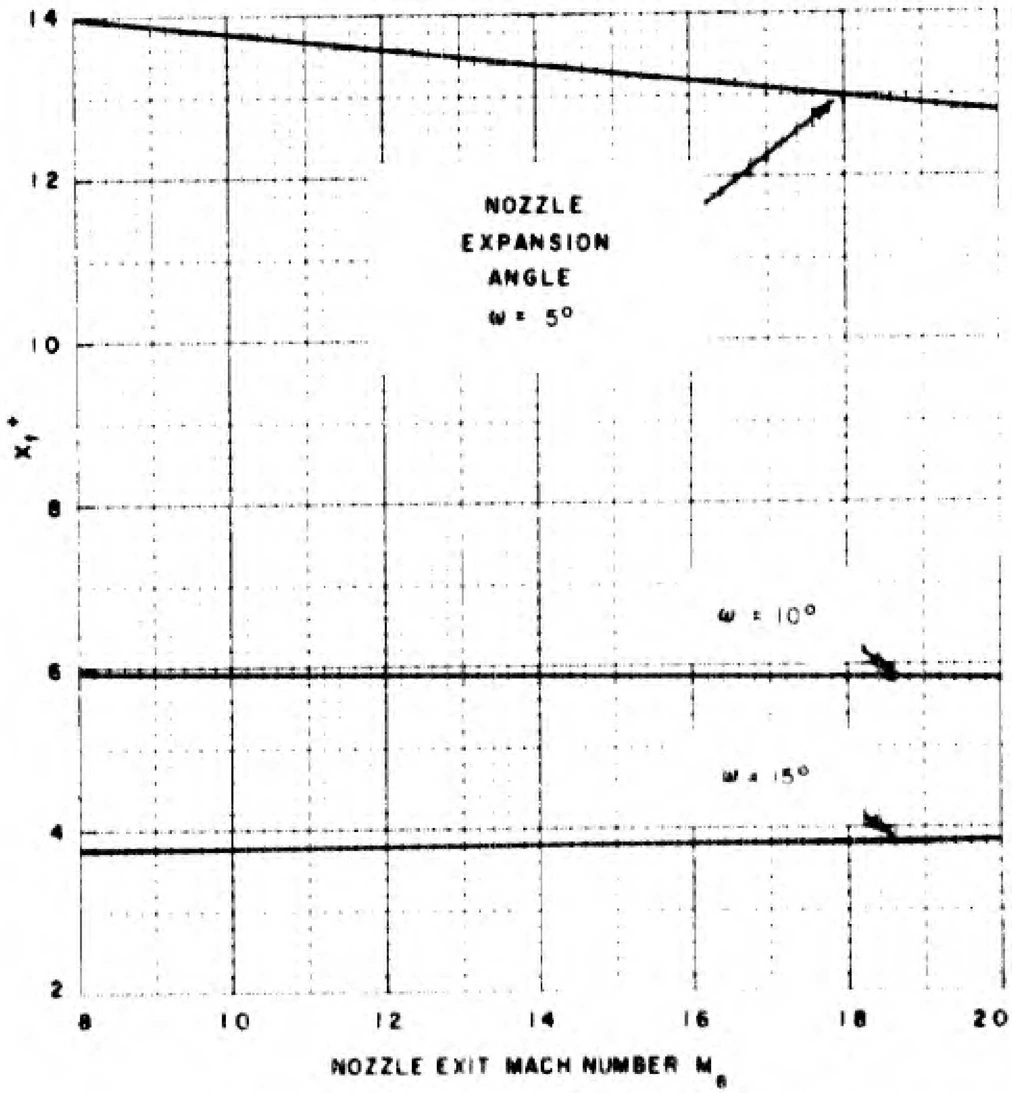

FIG 12 FOELSCH NOZZLE, DIMENSIONLESS LENGTH X_1^*

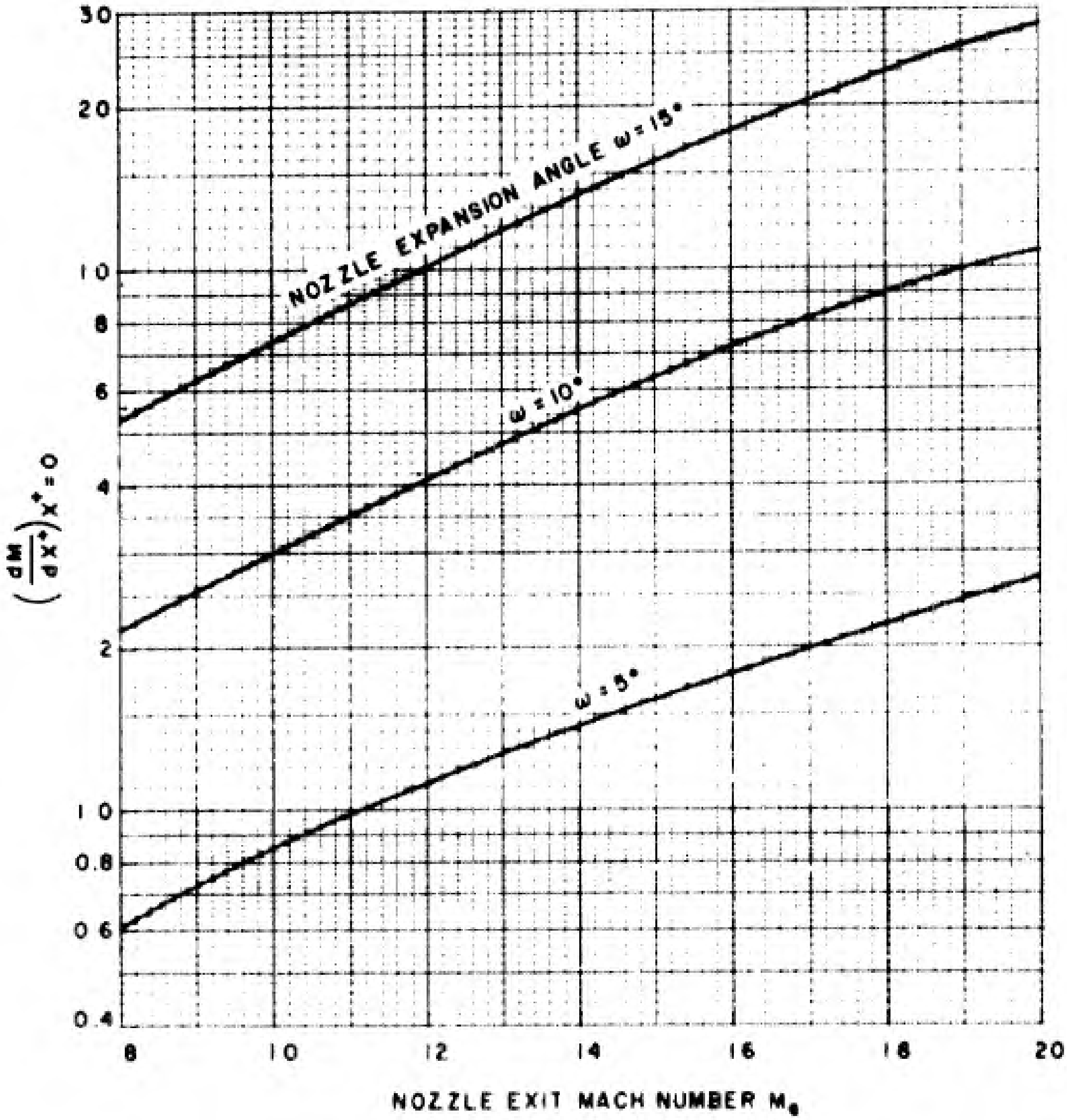

FIG 13 FOELSCH NOZZLE, DIMENSIONLESS THROAT MACH NUMBER GRADIENT

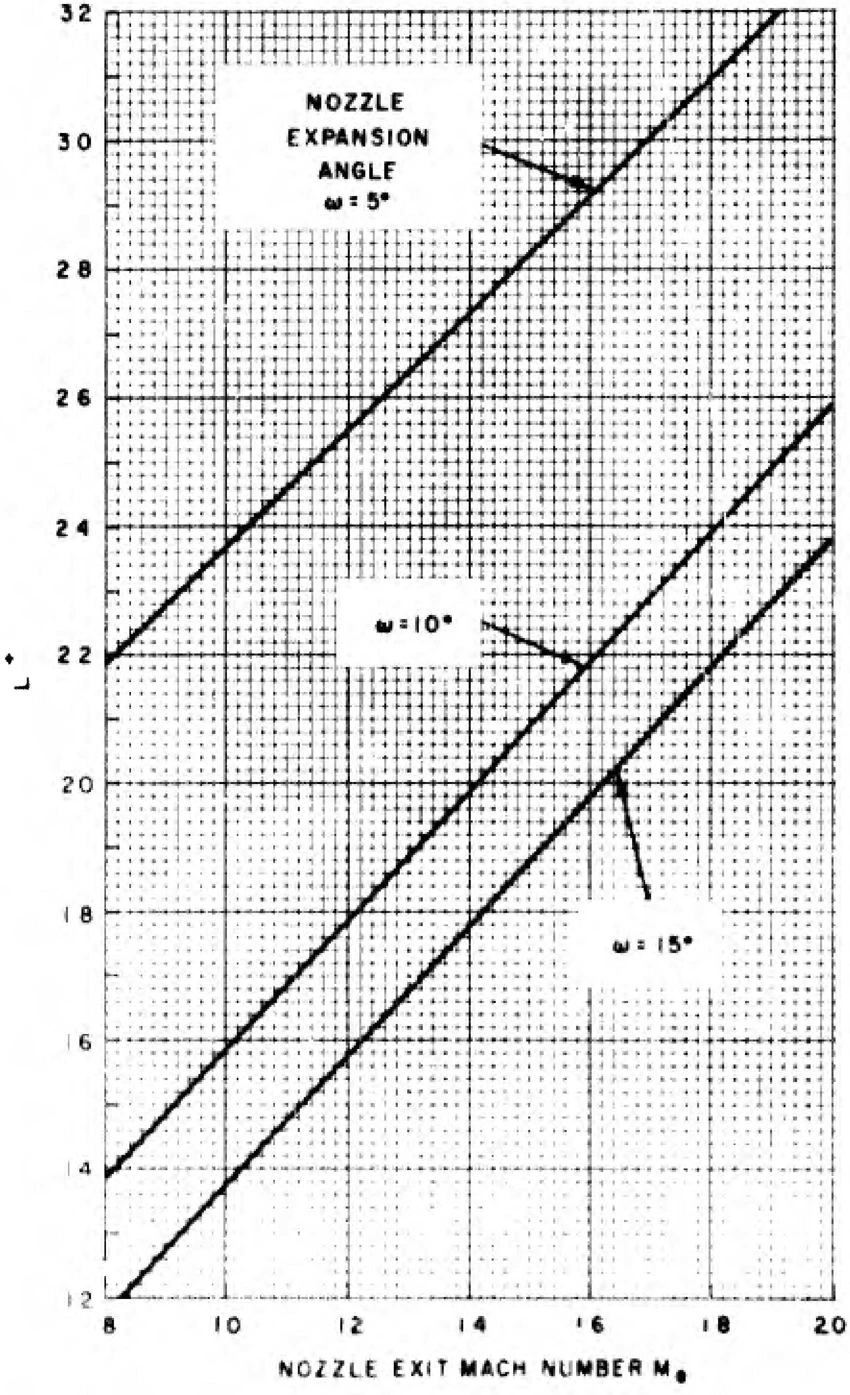

FIG 14 FOELSCH NOZZLE, DIMENSIONLESS THROAT-EXIT LENGTH

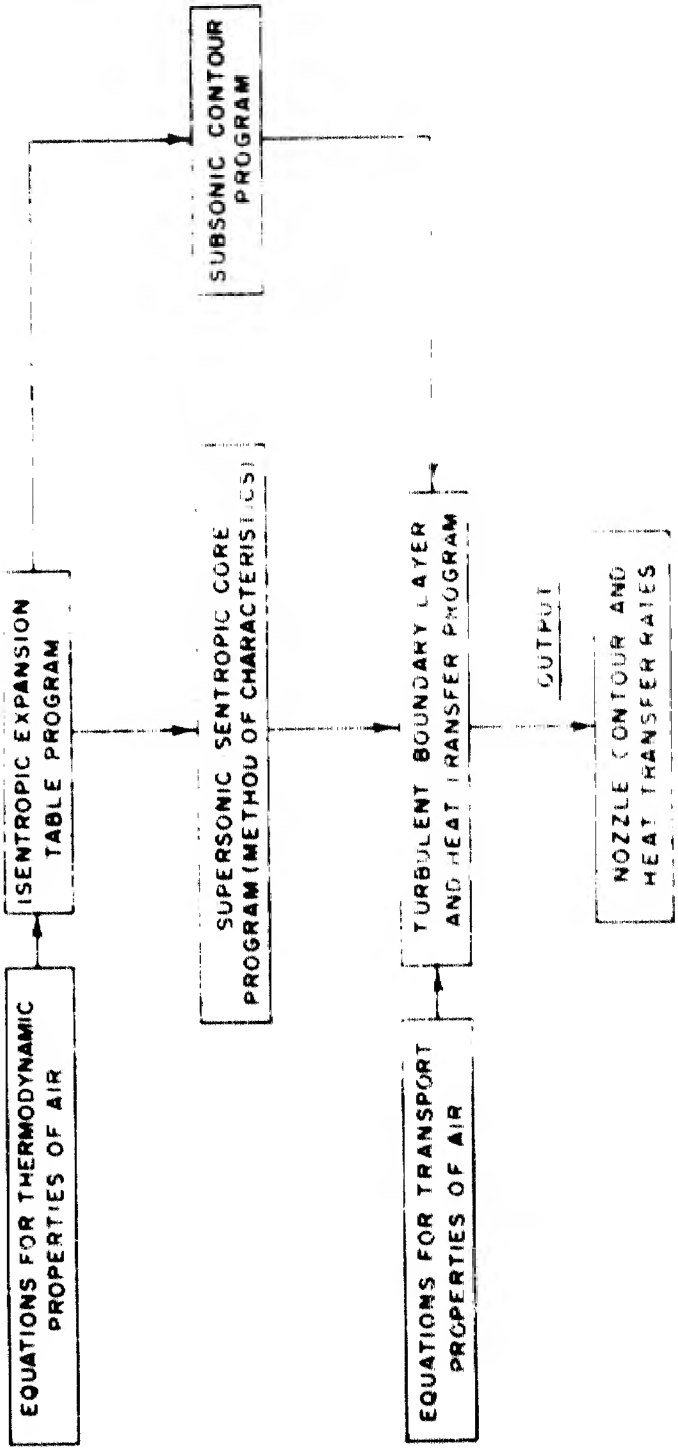

FIG 15 FLOW CHART OF COMPUTER PROGRAMS

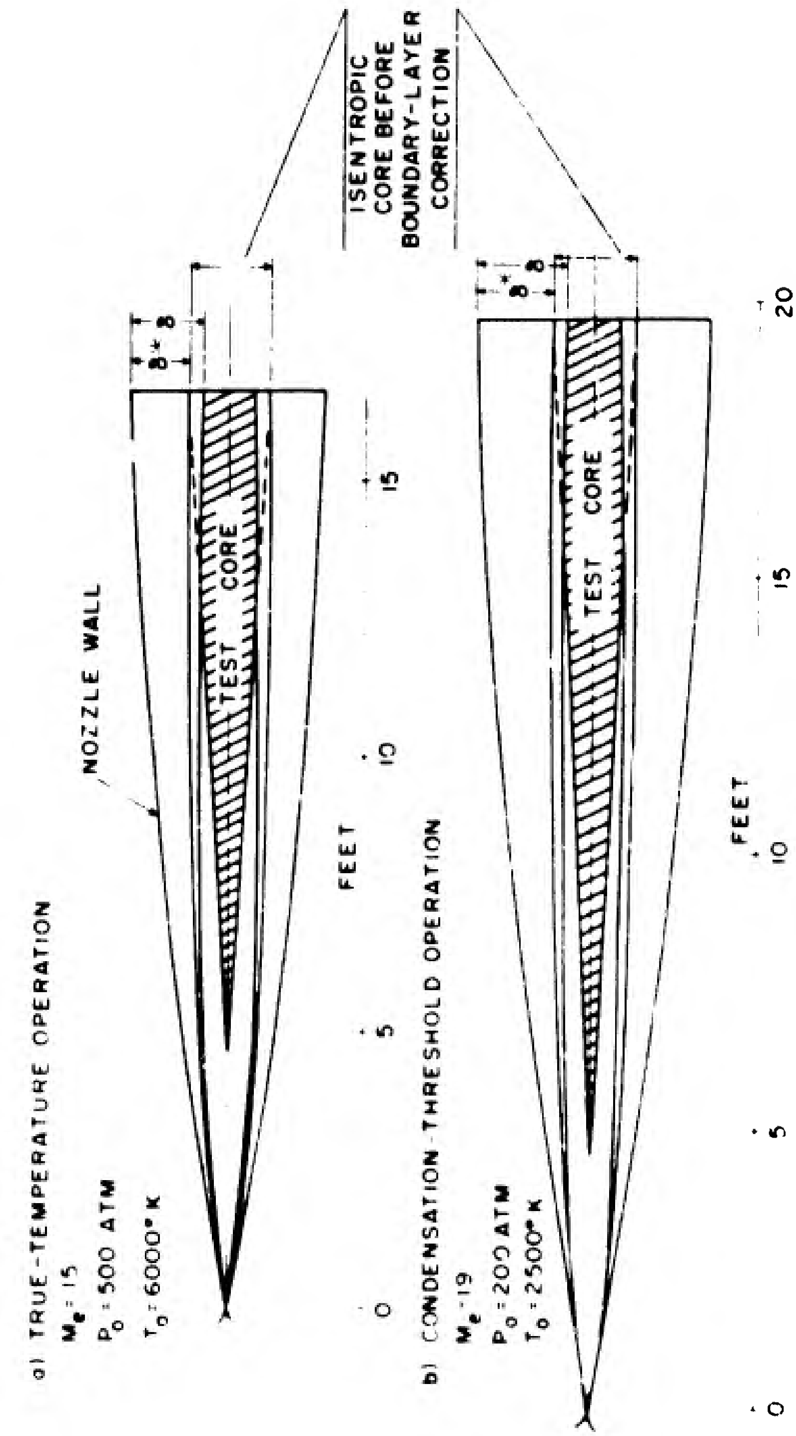

FIG 16 REPRESENTATIVE NOZZLE CONTOURS

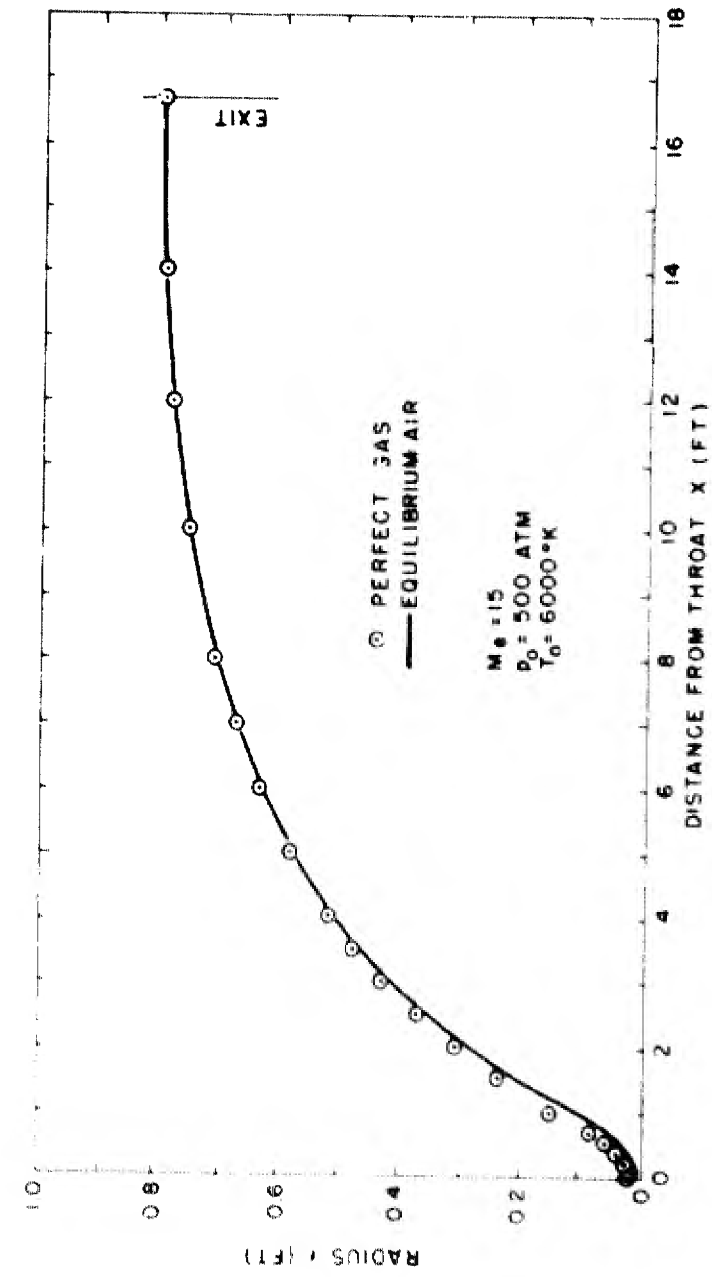

FIG 17 COMPARISON OF PERFECT-GAS AND EQUILIBRIUM-AIR ISENTROPIC CORE CONTOURS

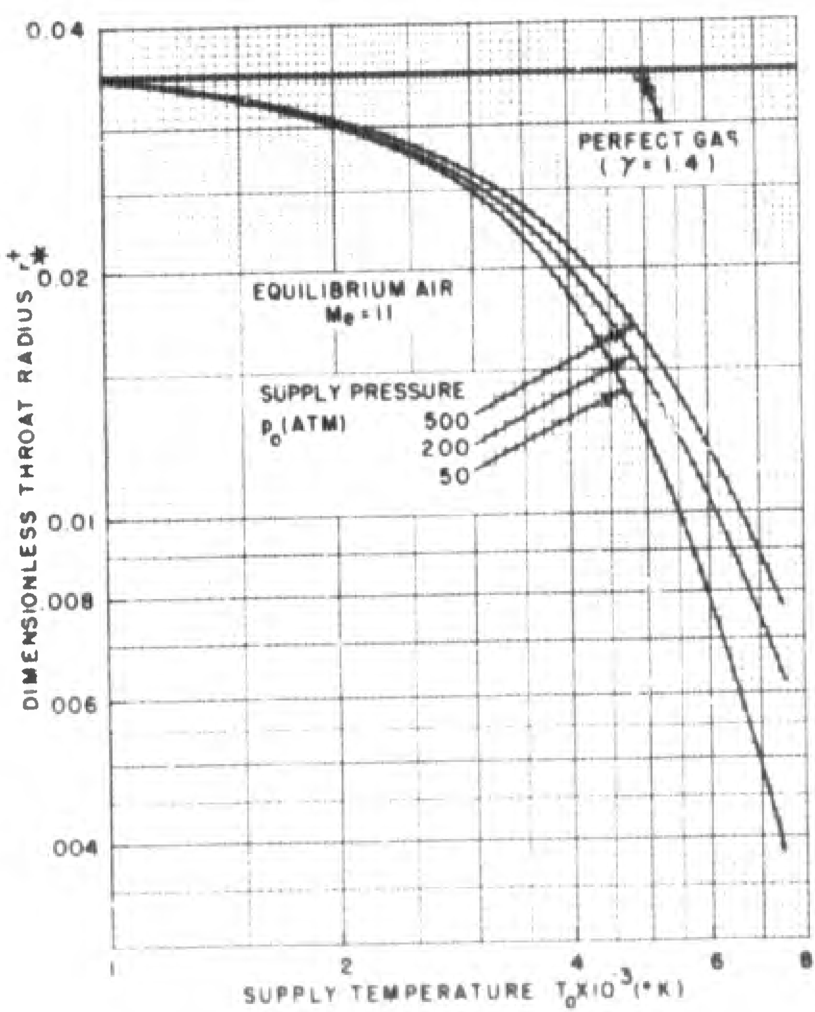

FIG 18 EFFECT OF SUPPLY CONDITIONS ON THROAT SIZE OF MACH 11 NOZZLE

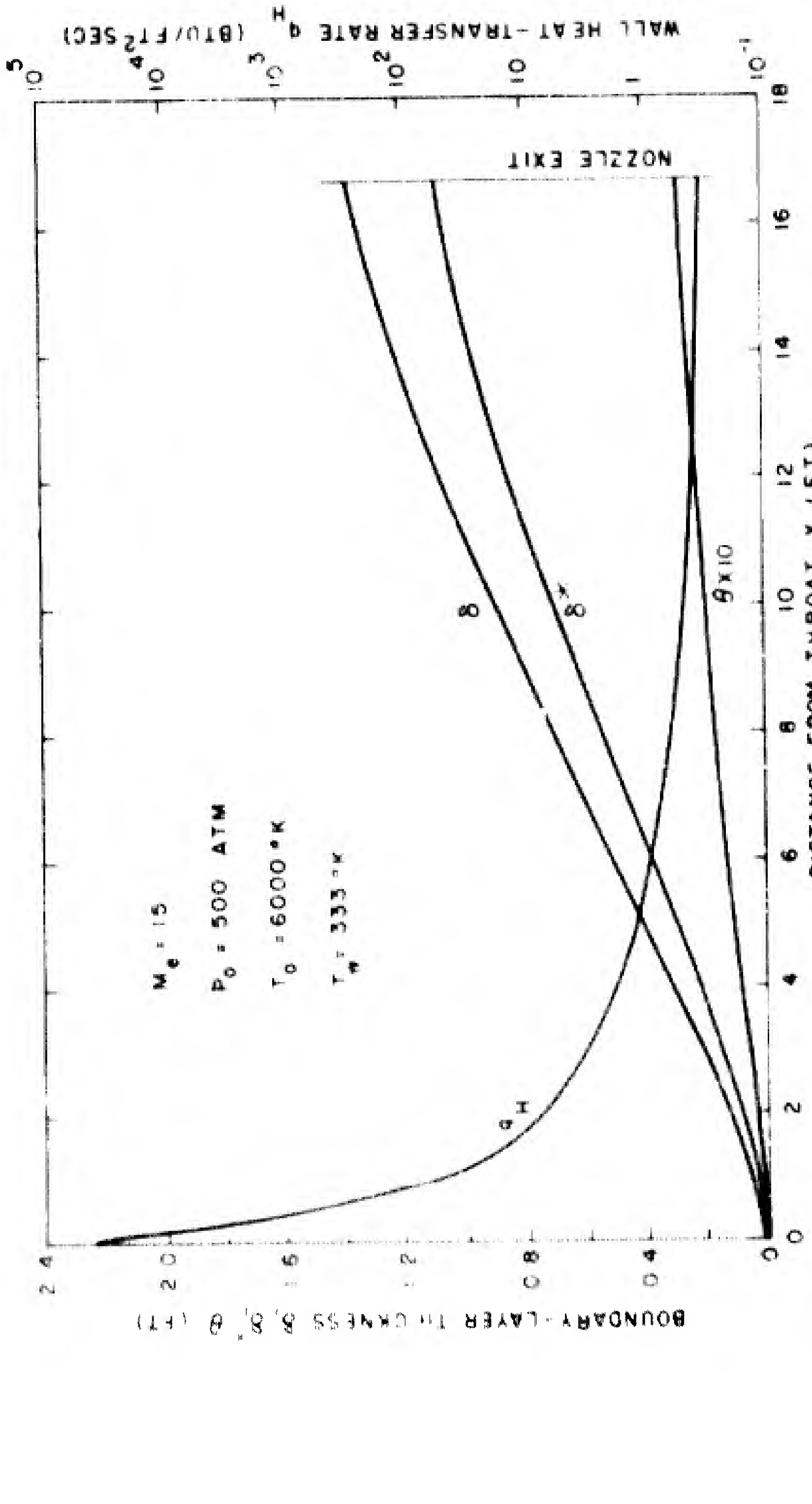

FIG 19 BOUNDARY-LAYER GROWTH AND CONVECTIVE HEAT-TRANSFER RATE IN MACH 15 NOZZLE

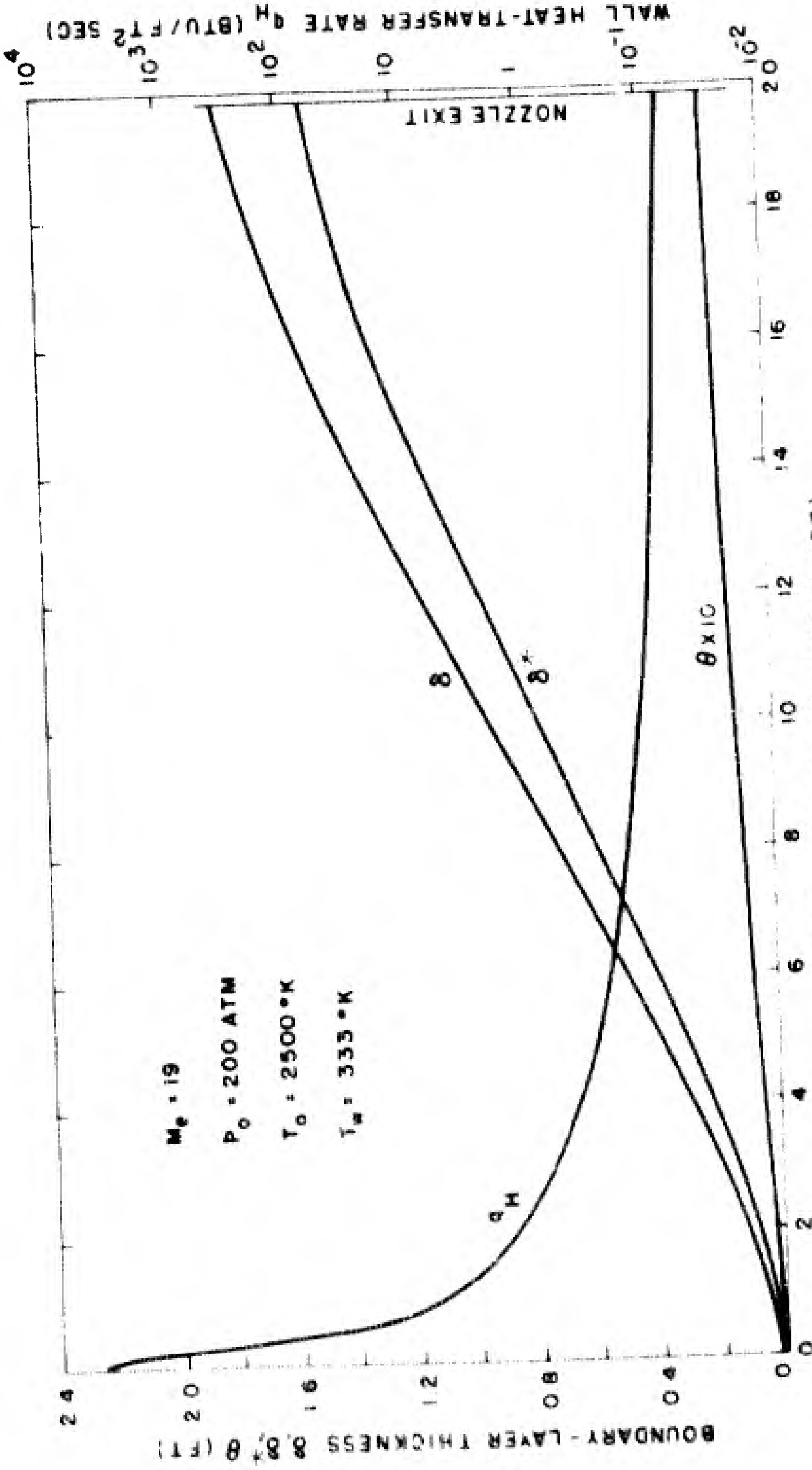

FIG 20 BOUNDARY LAYER GROWTH AND CONVECTIVE HEAT-TRANSFER RATE IN MACH 19 NOZZLE

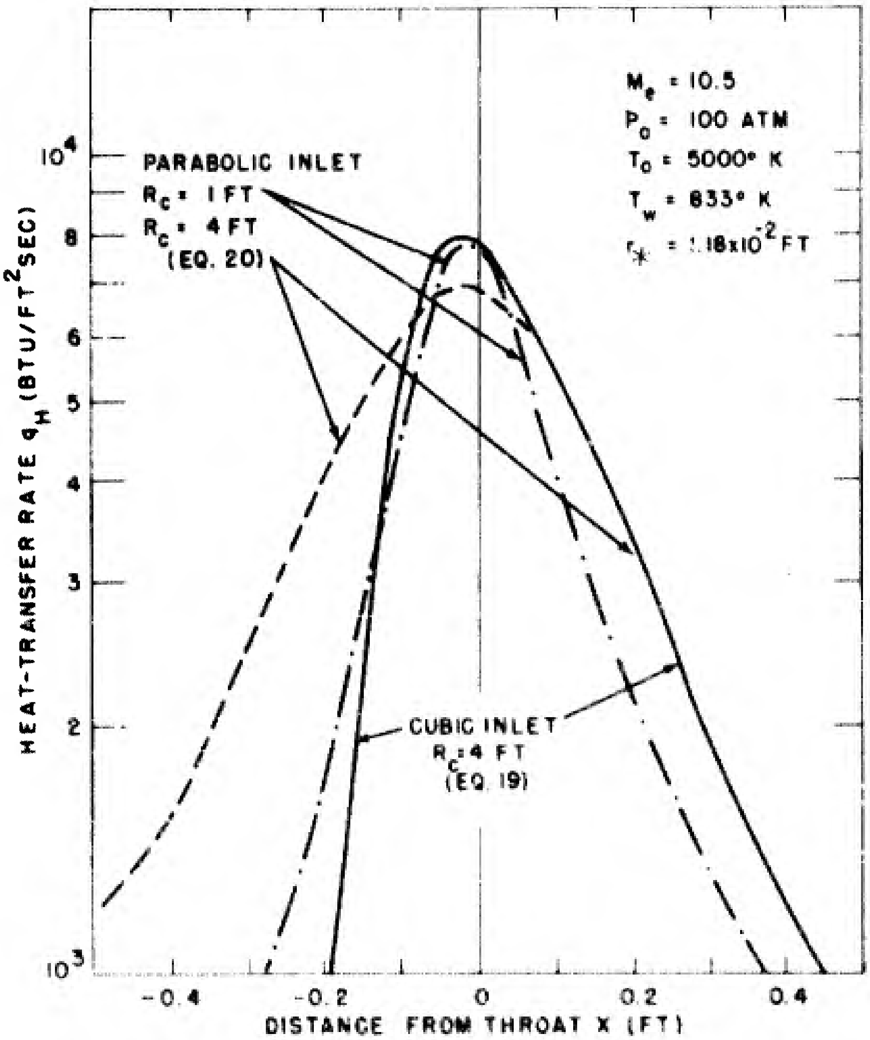

FIG. 21 EFFECT OF NOZZLE INLET GEOMETRY ON CONVECTIVE HEAT-TRANSFER RATE

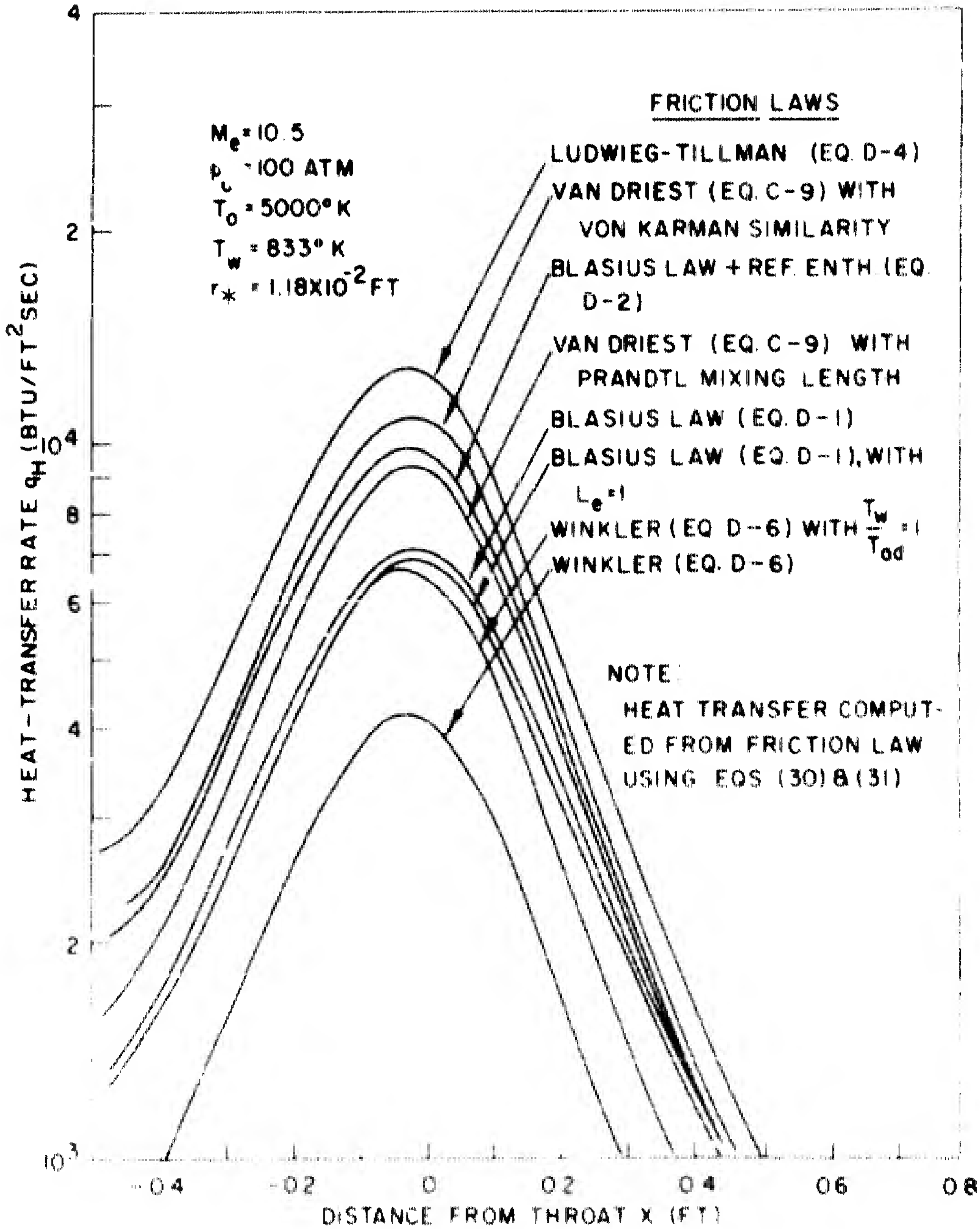

FIG 22 EFFECT OF FRICTION LAW ON CONVECTIVE THROAT HEATING

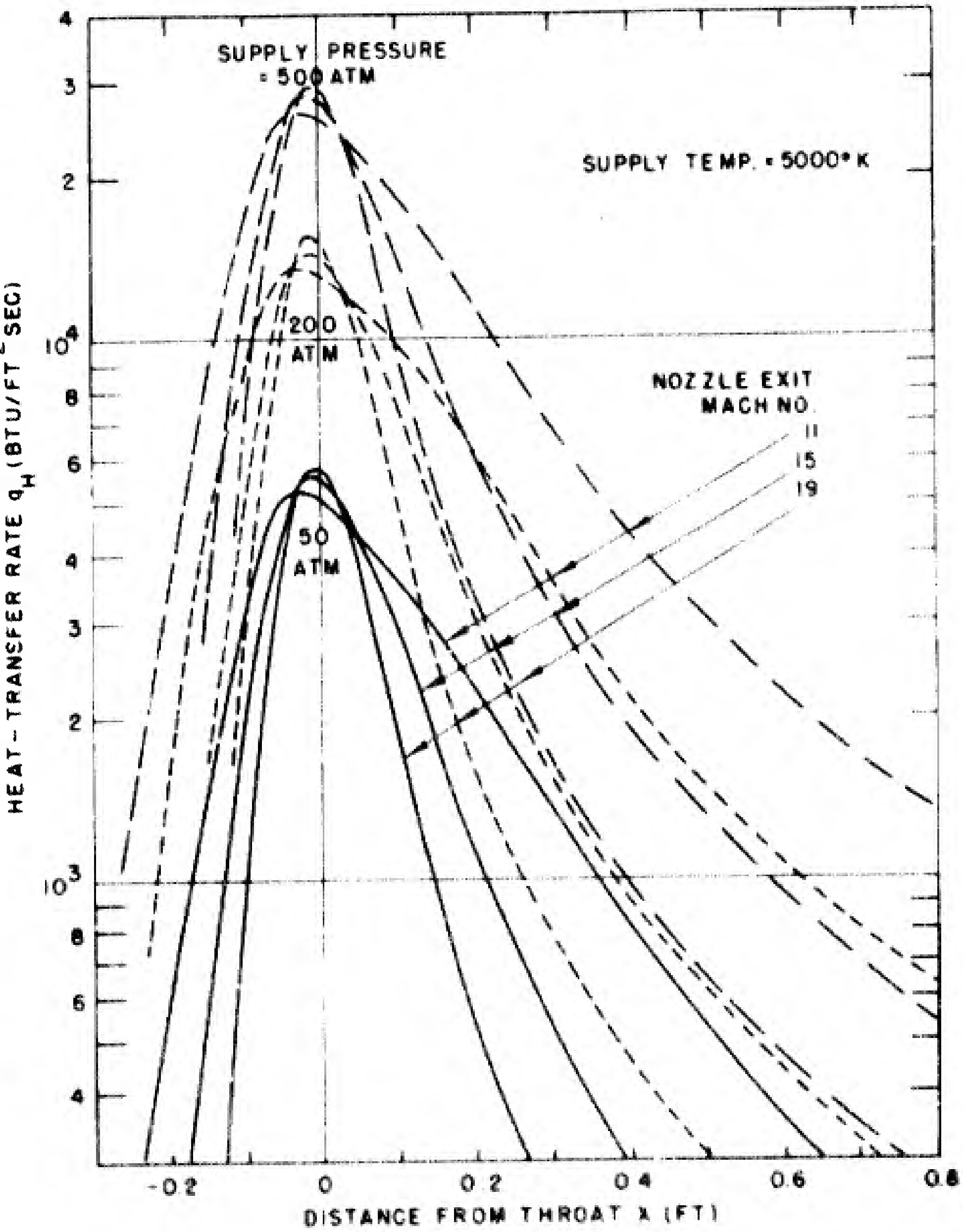

FIG. 23 VARIATION OF HEAT-TRANSFER RATE IN THE THROAT REGION FOR A FAMILY OF NOZZLES

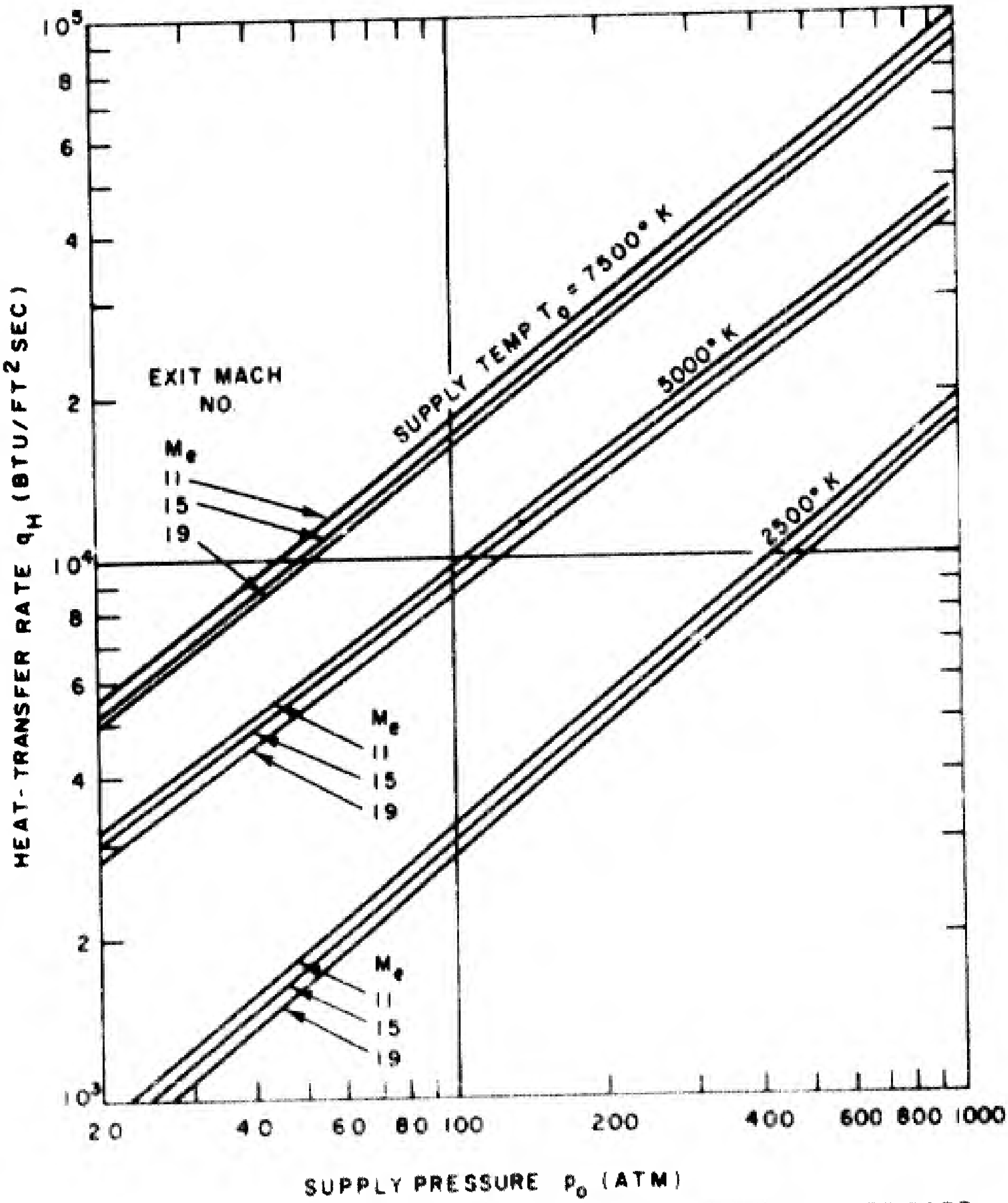

FIG 24 PEAK NOZZLE THROAT CONVECTIVE HEAT-TRANSFER RATE

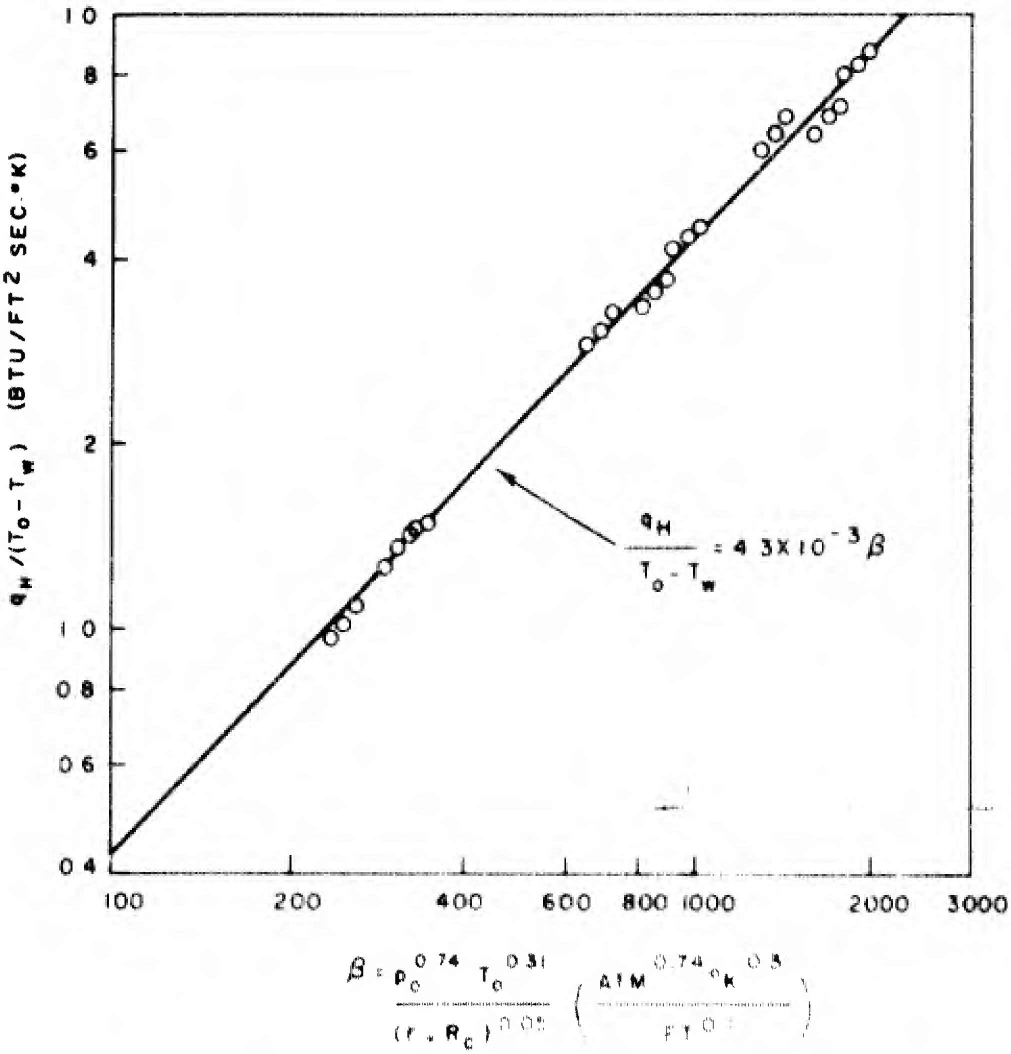

FIG 25 CORRELATION OF PEAK CONVECTIVE HEAT - TRANSFER RATE

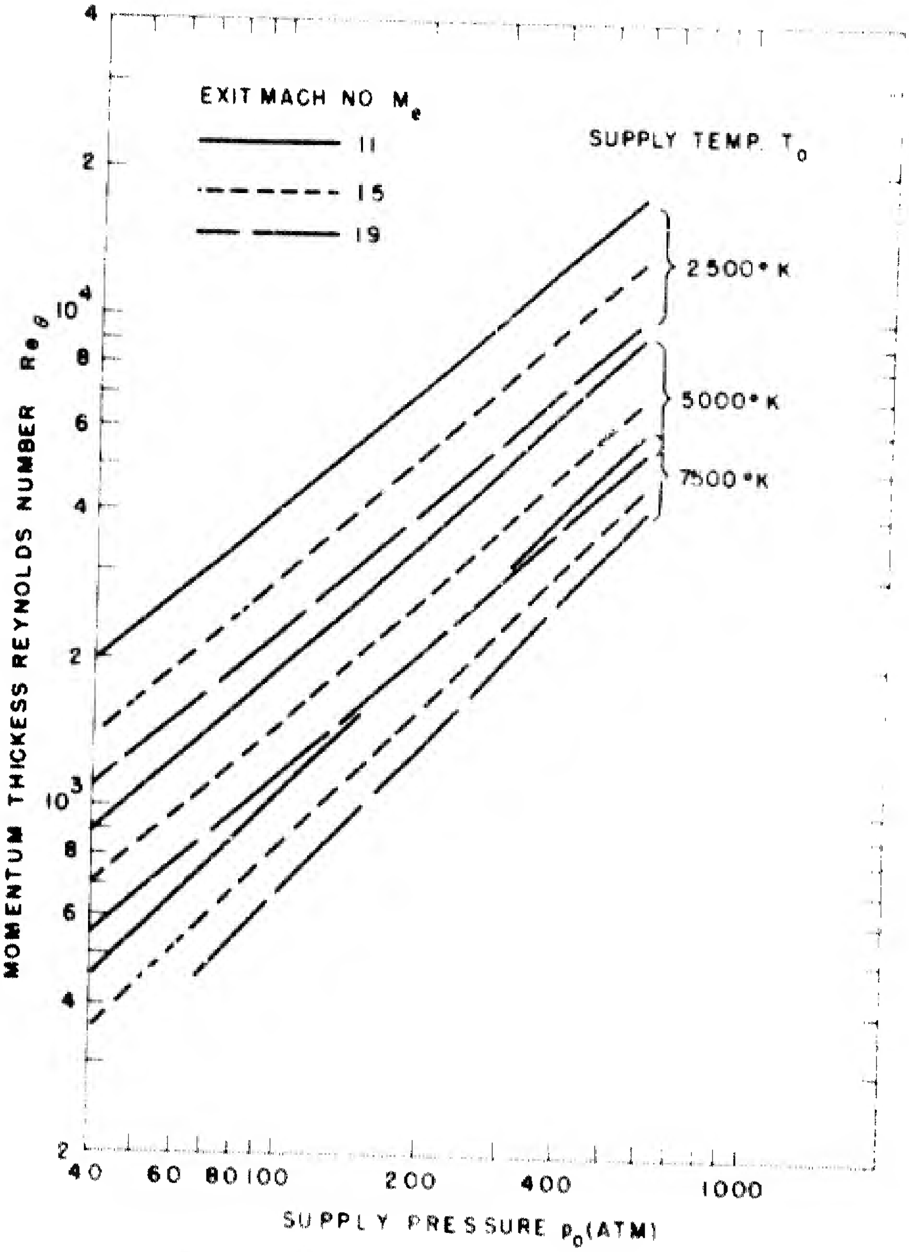

FIG 26 THROAT VALUE OF BOUNDARY-LAYER MOMENTUM THICKNESS REYNOLDS NUMBER

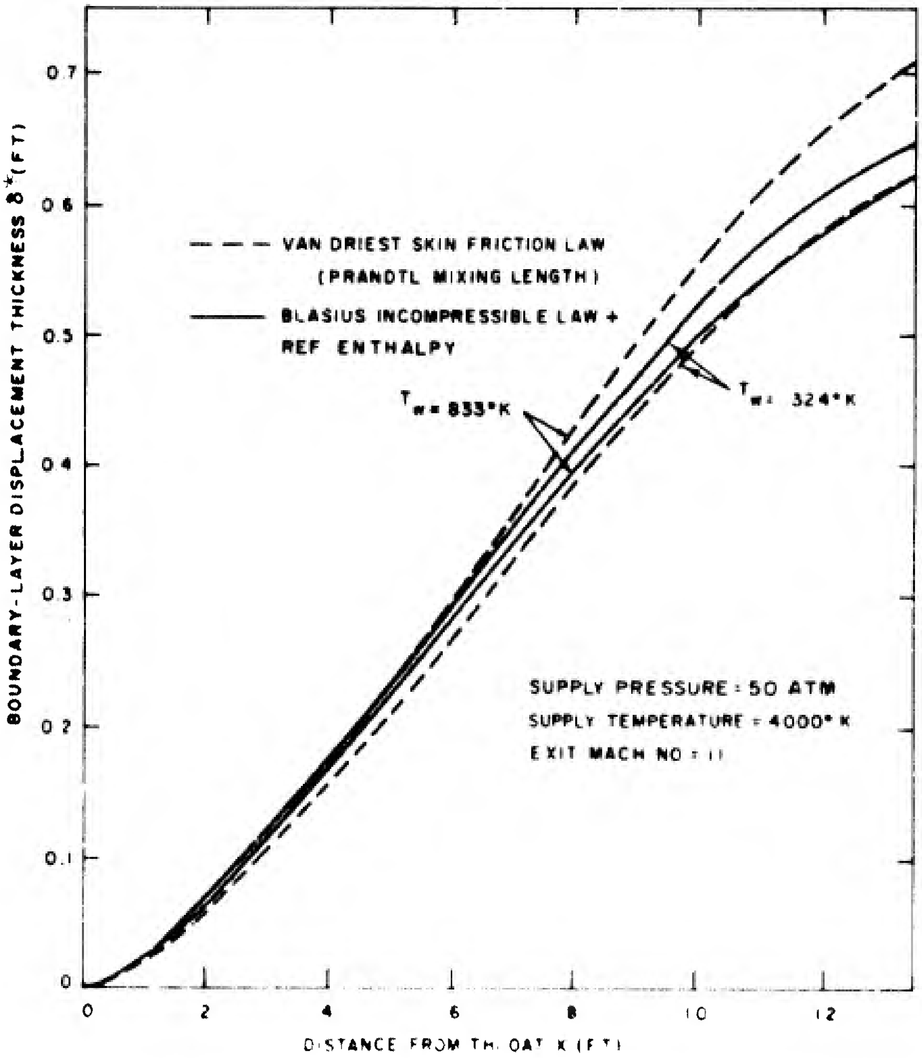

FIG 27 EFFECT OF FRICTION LAW ON NOZZLE BOUNDARY-LAYER GROWTH

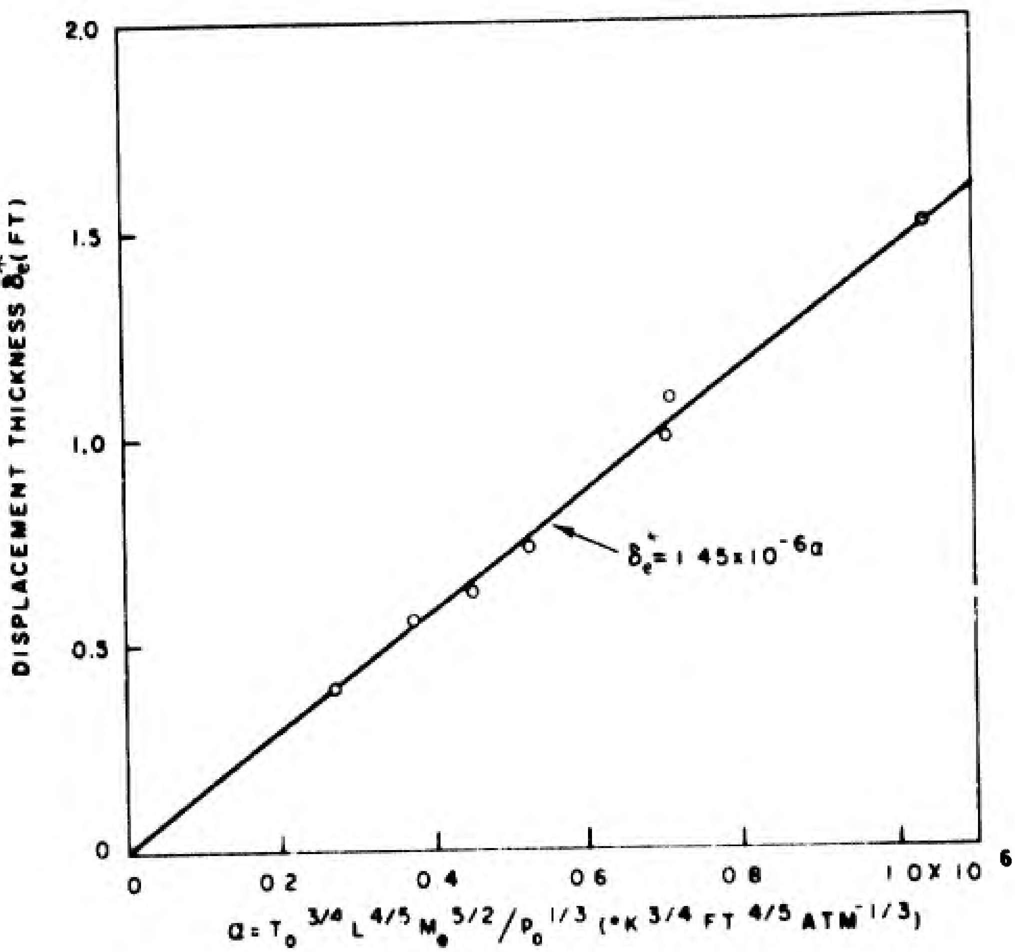

FIG. 28 CORRELATION OF NOZZLE EXIT BOUNDARY-LAYER DISPLACEMENT THICKNESS

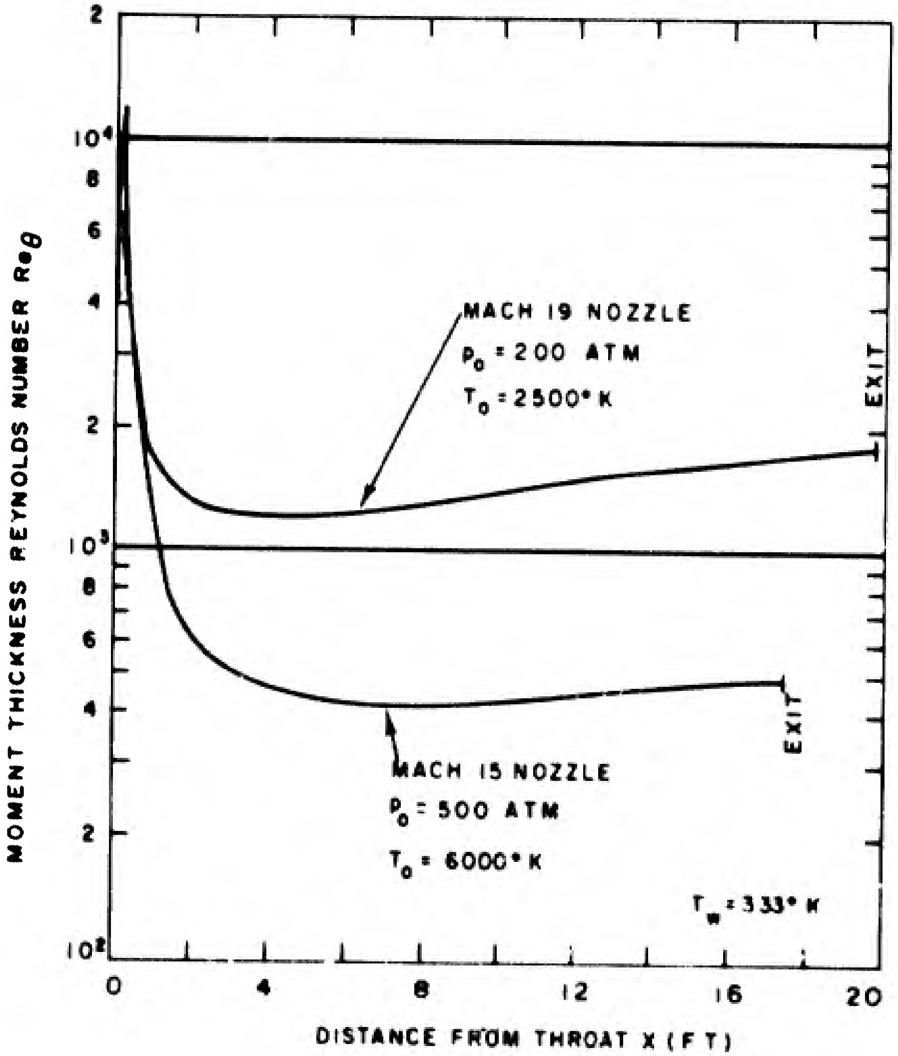

FIG 29 VARIATION OF MOMENTUM THICKNESS REYNOLDS NUMBER ALONG NOZZLE CONTOURS

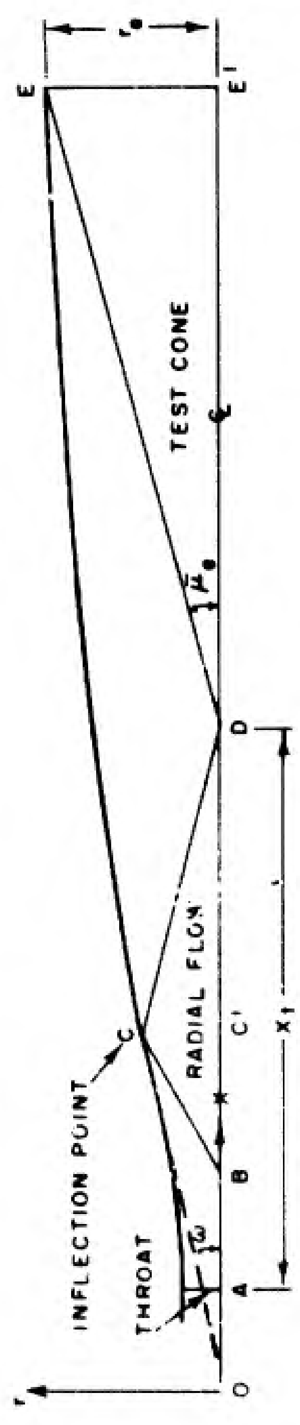

FIG 30 GEOMETRY OF THE FOELSCH NOZZLE

TABLE I

EXAMPLES OF HIGH-TEMPERATURE NOZZLES
Exit core area = 2 ft^2 (r_e = 0.7973 ft.)
Nominal half-expansion angle ω = 10°

Quantity	Symbol	Units	1	2	3	4	5	6	7
Exit Mach Number	M_e	-	11	11	15	19	15	15	15
Supply Pressure	p_o	atm.	50	200	500	200	500	500	200
Supply Temperature	T_o	°K	4000	4000	6000	2500	4000	2500	4000
Exit Static Pressure	p_e	mm Hg	0.143	0.853	0.078	0.029	0.271	0.511	0.083
Exit Static Temperature	T_e	°K	227	232	211	40.7	124	69.7	120
Throat-Exit Length	L	feet	13.48	13.48	16.68	19.83	16.68	16.68	16.68
Throat-Test Core Length	x_t	feet	4.74	4.74	4.72	4.69	4.72	4.72	4.72
Throat Core Radius	r^*	feet	1.48×10^{-2}	1.61×10^{-2}	4.58×10^{-3}	5.87×10^{-3}	8.11×10^{-3}	1.06×10^{-2}	7.64×10^{-3}
Throat Radius of Curvature*	R_c	feet	5.0	3.6	4.3	1.5	2.3	1.6	2.9
Half-Expansion Angle	ω	degrees	12.6	10.1	12.1	11.0	10.6	10.6	11.8
Exit Total B.L. Thickness	δ_e	feet	0.960	0.603	1.369	1.811	0.965	0.747	1.250
Exit Displacement Thickness	δ_e^*	feet	0.707	0.396	1.089	1.516	0.731	0.553	0.987
Exit Momentum Thickness	θ_e	feet	0.0275	0.0185	0.0278	0.0216	0.0180	0.0128	0.0231
Total Exit Dia.	$2(r_e+\delta_e^*)$	feet	3.010	2.388	3.774	4.628	3.058	2.702	3.570
Uniform Flow Dia.	$2(r_e+\delta_e^*-\delta_e)$	feet	1.090	1.182	1.036	1.006	1.128	1.208	1.070

*Value computed using equation (B-7), with γ = 1.4.

AERODYNAMICS DEPARTMENT
EXTERNAL DISTRIBUTION LIST (A1)

	No. of Copies
Chief, Bureau of Naval Weapons Department of the Navy Washington 25, D. C.	
Attn: DLI-30	1
Attn: R-14	1
Attn: RRRE-4	1
Attn: RMGA-413	1
Office of Naval Research Room 2709, T-3 Washington 25, D. C. Attn: Head, Mechanics Branch	1
Director, David Taylor Model Basin Aerodynamics Laboratory Washington 7, D. C. Attn: Library	1
Commander, U. S. Naval Ordnance Test Station China Lake, California	
Attn: Technical Library	1
Attn: Code 503	1
Attn: Code 406	1
Director, Naval Research Laboratory Washington 25, D. C. Attn: Code 2027	1
Commanding Officer Office of Naval Research Branch Office Box 39, Navy 100 Fleet Post Office New York, New York	1
NASA High Speed Flight Station Box 273 Edwards Air Force Base, California Attn: W. C. Williams	1
NASA Ames Research Center Moffett Field, California Attn: Librarian	1

AERODYNAMICS DEPARTMENT
EXTERNAL DISTRIBUTION LIST (A1)

	No. of Copies
NASA Langley Research Center Langley Field, Virginia	
Attn: Librarian	3
Attn: C. H. McLellan	1
Attn: J. J. Stack	1
Attn: Adolf Busemann	1
Attn: Comp. Res. Div.	1
Attn: Theoretical Aerodynamics Division	1
NASA Lewis Research Center 21000 Brookpark Road Cleveland 11, Ohio	
Attn: Librarian	1
Attn: Chief, Propulsion Aerodynamics Div.	1
NASA 1520 H Street, N. W. Washington 25, D. C.	
Attn: Chief, Division of Res. Information	1
Office of the Assistant Secretary of Defense (R&D) Room 3E1065, The Pentagon Washington 25, D. C.	
Attn: Technical Library	1
Research and Development Board Room 3D1041, The Pentagon Washington 25, D. C.	
Attn: Library	1
ASTIA Arlington Hall Station Arlington 12, Virginia	10
Commander, Pacific Missile Range Point Mugu, California	
Attn: Technical Library	1
Commanding General Aberdeen Proving Ground, Maryland	
Attn: Technical Information Branch	1
Attn: Ballistic Research Laboratory	1

AERODYNAMICS DEPARTMENT
EXTERNAL DISTRIBUTION LIST (A1)

	No. of Copies
Commander, Naval Weapons Laboratory Dahlgren, Virginia Attn: Library	1
Director, Special Projects Department of the Navy Washington 25, D. C. Attn: SP-2722	1
Director of Intelligence Headquarters, USAF Washington 25, D. C. Attn: AFOIN-3B	1
Headquarters - Aero. Systems Division Wright-Patterson Air Force Base Dayton, Ohio Attn: WWAD	2
Commander Air Force Ballistic Missile Division HQ Air Research & Development Command P. O. Box 262 Inglewood, California Attn: WDTLAR	1
Chief, Defense Atomic Support Agency Washington 25, D. C. Attn: Document Library	1
Headquarters, Arnold Engineering Development Center Air Research and Development Center Arnold Air Force Station, Tennessee Attn: Technical Library Attn: AEOR	1
Commanding Officer, DOFL Washington 25, D. C. Attn: Library, Room 211, Bldg. 92	1
Commanding General Redstone Arsenal Huntsville, Alabama Attn: Mr. N. Shapiro (ORDDW-MRF)	1

AERODYNAMICS DEPARTMENT
EXTERNAL DISTRIBUTION LIST (A1)

	No. of Copies
NASA George C. Marshall Space Flight Center Huntsville, Alabama	
Attn: Dr. E. Geissler	1
Attn: Mr. T. Reed	1
Attn: Mr. H. Paul	1
Attn: Mr. W. Dahm	1
Attn: Mr. D. Burrows	1
Attn: Mr. J. Kingsbury	1
Attn: ORDAB-DA	1
APL/JHU (C/NOw 7386) 8621 Georgia Avenue Silver Spring, Maryland	
Attn: Technical Reports Group	2
Attn: Mr. D. Fox	1
Attn: Dr. F. Hill	1
Via: INSORD	
Air Force Systems Command Scientific & Technical Liaison Office Room 2305, Munitions Building Department of the Navy Washington 25, D. C.	
Attn: E. G. Haas	1

AERODYNAMICS DEPARTMENT
EXTERNAL DISTRIBUTION LIST (A2)

	No. of Copies
Mr. J. Lukasiewicz Chief, Gas Dynamics Facility ARO, Incorporated Tullahoma, Tennessee	1
Massachusetts Institute of Technology Cambridge 39, Massachusetts	
Attn: Prof. J. Kaye	1
Attn: Prof. M. Finston	1
Attn: Mr. J. Baron	1
Polytechnic Institute of Brooklyn 527 Atlantic Avenue Freeport, New York	
Attn: Dr. A. Ferri	1
Attn: Dr. M. Bloom	1
Attn: Dr. P. Libby	1
Brown University Division of Engineering Providence, Rhode Island	
Attn: Prof. R. Probstein	1
Attn: Prof. C. Lin	1
University of Minnesota Minneapolis 14, Minnesota	
Attn: Dr. E. R. G. Eckert	1
Attn: Heat Transfer Laboratory	1
Attn: Technical Library	1
Rensselaer Polytechnic Institute Troy, New York	
Attn: Dept. of Aeronautical Engineering	1
Dr. James P. Hartnett Department of Mechanical Engineering University of Delaware Newark, Delaware	1
Princeton University James Forrestal Research Center Gas Dynamics Laboratory Princeton, New Jersey	
Attn: Prof. S. Bogdonoff	1

AERODYNAMICS DEPARTMENT
EXTERNAL DISTRIBUTION LIST (A2)

	No. of Copies
Institute for Fluid Dynamics and Applied Mathematics University of Maryland College Park, Maryland	
Attn: Director	2
Attn: Dr. J. Burgers	1
University of Michigan Ann Arbor, Michigan	
Attn: Dr. A. Kuethe	1
Applied Mathematics and Statistics Laboratory Stanford University Palo Alto, California	1
Cornell University Graduate School of Aeronautical Engineering Ithaca, New York	
Attn: Prof. W. R. Sears	1
The Johns Hopkins University Charles and 34th Streets Baltimore, Maryland	
Attn: Dr. F. H. Clauser	1
University of California Berkeley 4, California	
Attn: G. Maslach	1
Attn: Dr. S. Schaaf	1
Air Ballistics Laboratory Army Ballistic Missile Agency Huntsville, Alabama	1
Applied Mechanics Reviews Southwest Research Institute 8500 Culebra Road San Antonio 6, Texas	1
BuWepr Representative Aerojet-General Corporation 6352 N. Irwindale Avenue Azusa, California	1
Boeing Airplane Company Seattle, Washington	1

AERODYNAMICS DEPARTMENT
EXTERNAL DISTRIBUTION LIST (A2)

	No. of Copies
University of Minnesota Rosemount Research Laboratories Rosemount, Minnesota Attn: Technical Library	1
Director, Air University Library Maxwell Air Force Base, Alabama	1
Douglas Aircraft Company, Inc. Santa Monica Division 3000 Ocean Park Boulevard Santa Monica, California	
Attn: Chief Missiles Engineer	1
Attn: Aerodynamics Section	1
CONVAIR A Division of General Dynamics Corporation Daingerfield, Texas	1
CONVAIR Scientific Research Laboratory 5001 Kearney Villa Road San Diego 11, California	
Attn: Mr. M. Sibulkin	1
Attn: Asst. to the Director of Scientific Research	1
Attn: Dr. B. M. Leadon	1
Republic Aviation Corporation Farmingdale, New York Attn: Technical Library	1
General Applied Science Laboratories, Inc. Merrick and Stewart Avenues Westbury, L. I., New York	
Attn: Mr. Walter Daskin	1
Attn: Mr. R. W. B-rne	1
CONVAIR A Division of General Dynamics Corporation Fort Worth, Texas	1
Purdue University School of Aeronautical & Engineering Sciences LaFayette, Indiana Attn: R. L. Taggart, Library	1

AERODYNAMICS DEPARTMENT
EXTERNAL DISTRIBUTION LIST (A2)

	No. of Copies
United Aircraft Corporation 400 Main Street East Hartford 8, Connecticut	
Attn: Chief Librarian	1
Attn: Mr. W. Kuhrt, Research Dept.	2
Attn: Mr. J. G. Lee	1
Hughes Aircraft Company Florence Avenue at Teale Streets Culver City, California	
Attn: Mr. D. J. Johnson R&D Technical Library	1
McDonnell Aircraft Corporation P. O. Box 516 St. Louis 3, Missouri	1
Lockheed Aircraft Corporation Lockheed Missiles and Space Division Sunnyvale, California	
Attn: Dr. L. H. Wilson	1
Attn: Mr. M. Tucker	1
The Martin Company Baltimore 3, Maryland	
Attn: Library	1
Attn: Chief Aerodynamicist	1
North American Aviation, Inc. Aerophysics Laboratory Downing, California	
Attn: Dr. E. R. Van Driest	1
Department of Mechanical Engineering Yale University 400 Temple Street New Haven 10, Connecticut	
Attn: Dr. P. P. Wegener	1
MIT Lincoln Laboratory Lexington, Massachusetts	1
RAND Corporation 1700 Main Street Santa Monica, Claifornia	
Attn: Library, USAF Project RAND	1

AERODYNAMICS DEPARTMENT
EXTERNAL DISTRIBUTION LIST (A2)

	No. of Copies
Arnold Research Organization, Inc. Tullahoma, Tennessee	
Attn: Technical Library	1
Attn: Chief, Propulsion Wind Tunnel	1
Attn: Dr. J. Potter	1
General Electric Company Missile and Space Vehicle Department 3198 Chestnut Street Philadelphia, Pennsylvania	
Attn: Larry Chasen, Mgr. Library	2
Attn: Mr. R. Kirby	1
Attn: Dr. J. Farber	1
Attn: Dr. G. Sutton	1
Attn: Dr. J. D. Stewart	1
Attn: Dr. S. M. Scala	1
Attn: Dr. H. Lew	1
Eastman Kodak Company Navy Ordnance Division 50 West Main Street Rochester 14, New York	
Attn: W. B. Forman	2
Library AVCO-Everett Research Laboratory 2385 Revere Beach Parkway Everett 49, Massachusetts	3
AER, Incorporated 158 North Hill Avenue Pasadena, California	1
Armour Research Foundation 10 West 35th Street Chicago 16, Illinois	
Attn: Dept. M	2
Chance-Vought Aircraft, Inc. Dallas, Texas	
Attn: Librarian	2
Cornell Aeronautical Laboratory, Inc. 4455 Genesee Street Buffalo 21, New York	
Attn: Librarian	1
Attn: Dr. Franklin Moore	1

AERODYNAMICS DEPARTMENT
EXTERNAL DISTRIBUTION LIST (A2)

	No. of Copies
Defense Research Laboratory The University of Texas P. O. Box 8029 Austin 12, Texas	
Attn: Assistant Director	1
Ohio State University Columbus 10, Ohio	
Attn: Security Officer	1
Attn: Aerodynamics Laboratory	1
Attn: Dr. J. Lee	1
Attn: Chairman, Dept. of Aero. Engr.	1
California Institute of Technology Pasadena, California	
Attn: Guggenheim Aeronautical Laboratory, Aeronautics Library	1
Attn: Jet Propulsion Laboratory	1
Attn: Dr. H. Liepmann	1
Attn: Dr. L. Lees	1
Attn: Dr. D. Coles	1
Attn: Mr. A. Roshko	1
Case Institute of Technology Cleveland 6, Ohio	
Attn: G. Kuerti	1
Superintendent U. S. Naval Postgraduate School Monterey, California	
Attn: Technical Reports Section Library	1
National Bureau of Standards Washington 25, D. C.	
Attn: Chief, Fluid Mechanics Section	1

Naval Ordnance Laboratory, White Oak, Md.
(NAVWEPS report 7395)
THE AERODYNAMIC DESIGN OF AXISYMMETRIC NOZZLES FOR HIGH-TEMPERATURE AIR, by K.R. Enkenhus and E.F. Maher. 5 Feb. 1962. 38p. charts, tables. (Aeroballistics research report 137). Task PR-10. UNCLASSIFIED

A method is given for aerodynamic design of contoured axisymmetric nozzles by the method of characteristics, with a turbulent boundary-layer correction, for high-temperature air in thermodynamic equilibrium.

The method has been coded on an IBM 704 computer, and used to investigate boundary-layer growth and heat transfer in a family of hypervelocity nozzles having exit Mach numbers from 11 to 19, supply pressures from 50 to 500 atmospheres and supply temperatures up to 7500°K.

1. Nozzles - Aerodynamics
2. Nozzles, Axisymmetric
3. Nozzles - Boundary layer
4. Nozzles - Heat transfer
5. Computers - IBM 704

I. Title
II. Enkenhus, Kurt R.
III. Maher, Edward F., jt. author
IV. Series
V. Project

Naval Ordnance Laboratory, White Oak, Md.
(NAVWEPS report 7395)
THE AERODYNAMIC DESIGN OF AXISYMMETRIC NOZZLES FOR HIGH-TEMPERATURE AIR, by K.R. Enkenhus and E.F. Maher. 5 Feb. 1962. 38p. charts, tables. (Aeroballistics research report 137). Task PR-10. UNCLASSIFIED

A method is given for aerodynamic design of contoured axisymmetric nozzles by the method of characteristics, with a turbulent boundary-layer correction, for high-temperature air in thermodynamic equilibrium.

The method has been coded on an IBM 704 computer, and used to investigate boundary-layer growth and heat transfer in a family of hypervelocity nozzles having exit Mach numbers from 11 to 19, supply pressures from 50 to 500 atmospheres and supply temperatures up to 7500°K.

1. Nozzles - Aerodynamics
2. Nozzles, Axisymmetric
3. Nozzles - Boundary layer
4. Nozzles - Heat transfer
5. Computers - IBM 704

I. Title
II. Enkenhus, Kurt R.
III. Maher, Edward F., jt. author
IV. Series
V. Project

Naval Ordnance Laboratory, White Oak, Md.
(NAVWEPS report 7395)
THE AERODYNAMIC DESIGN OF AXISYMMETRIC NOZZLES FOR HIGH-TEMPERATURE AIR, by K.R. Enkenhus and E.F. Maher. 5 Feb. 1962. 38p. charts, tables. (Aeroballistics research report 137). Task PR-10. UNCLASSIFIED

A method is given for aerodynamic design of contoured axisymmetric nozzles by the method of characteristics, with a turbulent boundary-layer correction, for high-temperature air in thermodynamic equilibrium.

The method has been coded on an IBM 704 computer, and used to investigate boundary-layer growth and heat transfer in a family of hypervelocity nozzles having exit Mach numbers from 11 to 19, supply pressures from 50 to 500 atmospheres and supply temperatures up to 7500°K.

1. Nozzles - Aerodynamics
2. Nozzles, Axisymmetric
3. Nozzles - Boundary layer
4. Nozzles - Heat transfer
5. Computers - IBM 704

I. Title
II. Enkenhus, Kurt R.
III. Maher, Edward F., jt. author
IV. Series
V. Project

Naval Ordnance Laboratory, White Oak, Md.
(NAVWEPS report 7395)
THE AERODYNAMIC DESIGN OF AXISYMMETRIC NOZZLES FOR HIGH-TEMPERATURE AIR, by K.R. Enkenhus and E.F. Maher. 5 Feb. 1962. 38p. charts, tables. (Aeroballistics research report 137). Task PR-10. UNCLASSIFIED

A method is given for aerodynamic design of contoured axisymmetric nozzles by the method of characteristics, with a turbulent boundary-layer correction, for high-temperature air in thermodynamic equilibrium.

The method has been coded on an IBM 704 computer, and used to investigate boundary-layer growth and heat transfer in a family of hypervelocity nozzles having exit Mach numbers from 11 to 19, supply pressures from 50 to 500 atmospheres and supply temperatures up to 7500°K.

1. Nozzles - Aerodynamics
2. Nozzles, Axisymmetric
3. Nozzles - Boundary layer
4. Nozzles - Heat transfer
5. Computers - IBM 704

I. Title
II. Enkenhus, Kurt R.
III. Maher, Edward F., jt. author
IV. Series
V. Project

Naval Ordnance Laboratory, White Oak, Md.
(NAVWEPS report 7395)
THE AERODYNAMIC DESIGN OF AXISYMMETRIC NOZZLES FOR HIGH-TEMPERATURE AIR, by K.R. Enkenhus and E.F. Maher. 5 Feb. 1962. 38p. charts, tables. (Aeroballistics research report 137). Task FR-10. UNCLASSIFIED

A method is given for aerodynamic design of contoured axisymmetric nozzles by the method of characteristics, with a turbulent boundary-layer correction, for high-temperature air in thermodynamic equilibrium.

The method has been coded on an IBM 704 computer, and used to investigate boundary-layer growth and heat transfer in a family of hypervelocity nozzles having exit Mach numbers from 11 to 19, supply pressures from 50 to 500 atmospheres and supply temperatures up to 7500°R.

1. Nozzles - Aerodynamics
2. Nozzles, Axisymmetric
3. Nozzles - Boundary layer
4. Nozzles - Heat transfer
5. Computers - IBM 704

I. Title
II. Enkenhus, Kurt R.
III. Maher, Edward F., jt. author
IV. Series
V. Project

Naval Ordnance Laboratory, White Oak, Md.
(NAVWEPS report 7395)
THE AERODYNAMIC DESIGN OF AXISYMMETRIC NOZZLES FOR HIGH-TEMPERATURE AIR, by K.R. Enkenhus and E.F. Maher. 5 Feb. 1962. 38p. charts, tables. (Aeroballistics research report 137). Task FR-10. UNCLASSIFIED

A method is given for aerodynamic design of contoured axisymmetric nozzles by the method of characteristics, with a turbulent boundary-layer correction, for high-temperature air in thermodynamic equilibrium.

The method has been coded on an IBM 704 computer, and used to investigate boundary-layer growth and heat transfer in a family of hypervelocity nozzles having exit Mach numbers from 11 to 19, supply pressures from 50 to 500 atmospheres and supply temperatures up to 7500°R.

1. Nozzles - Aerodynamics
2. Nozzles, Axisymmetric
3. Nozzles - Boundary layer
4. Nozzles - Heat transfer
5. Computers - IBM 704

I. Title
II. Enkenhus, Kurt R.
III. Maher, Edward F., jt. author
IV. Series
V. Project

Naval Ordnance Laboratory, White Oak, Md.
(NAVWEPS report 7395)
THE AERODYNAMIC DESIGN OF AXISYMMETRIC NOZZLES FOR HIGH-TEMPERATURE AIR, by K.R. Enkenhus and E.F. Maher. 5 Feb. 1962. 38p. charts, tables. (Aeroballistics research report 137). Task FR-10. UNCLASSIFIED

A method is given for aerodynamic design of contoured axisymmetric nozzles by the method of characteristics, with a turbulent boundary-layer correction, for high-temperature air in thermodynamic equilibrium.

The method has been coded on an IBM 704 computer, and used to investigate boundary-layer growth and heat transfer in a family of hypervelocity nozzles having exit Mach numbers from 11 to 19, supply pressures from 50 to 500 atmospheres and supply temperatures up to 7500°R.

1. Nozzles - Aerodynamics
2. Nozzles, Axisymmetric
3. Nozzles - Boundary layer
4. Nozzles - Heat transfer
5. Computers - IBM 704

I. Title
II. Enkenhus, Kurt R.
III. Maher, Edward F., jt. author
IV. Series
V. Project

Naval Ordnance Laboratory, White Oak, Md.
(NAVWEPS report 7395)
THE AERODYNAMIC DESIGN OF AXISYMMETRIC NOZZLES FOR HIGH-TEMPERATURE AIR, by K.R. Enkenhus and E.F. Maher. 5 Feb. 1962. 38p. charts, tables. (Aeroballistics research report 137). Task FR-10. UNCLASSIFIED

A method is given for aerodynamic design of contoured axisymmetric nozzles by the method of characteristics, with a turbulent boundary-layer correction, for high-temperature air in thermodynamic equilibrium.

The method has been coded on an IBM 704 computer, and used to investigate boundary-layer growth and heat transfer in a family of hypervelocity nozzles having exit Mach numbers from 11 to 19, supply pressures from 50 to 500 atmospheres and supply temperatures up to 7500°R.

1. Nozzles - Aerodynamics
2. Nozzles, Axisymmetric
3. Nozzles - Boundary layer
4. Nozzles - Heat transfer
5. Computers - IBM 704

I. Title
II. Enkenhus, Kurt R.
III. Maher, Edward F., jt. author
IV. Series
V. Project

UNCLASSIFIED

END

UNCLASSIFIED